Berechnung von Absorptionsspektren von Methan in Nicht-Gleichgewichts-Atmosphärendruckplasmen

Calculation of Absorption Spectra of Methane in Non-Equilibrium Atmospheric Pressure Plasmas

Bachelorarbeit

im
Studiengang
„Bachelor of Science“
im Fach Physik

an der Fakultät für Physik und Astronomie
der Ruhr-Universität Bochum

von

Thilo Romba

aus
Essen

Bochum 2018

Abstract

Durch die hohe Elektronentemperatur in Nicht-Gleichgewichts-Plasmen können bereits bei niedrigen Temperaturen chemische Reaktionen stattfinden, deren Aktivierungstemperatur deutlich über der Temperatur des Plasmas liegt. Durch diese Eigenschaft der Nicht-Gleichgewichts-Plasmen kann in diesen die chemische Konversion von Molekülen bei vergleichbar niedrigem Energieaufwand durchgeführt werden.
Die Dichten und Temperaturen von Plasmen mit verschiedenen CH_4 Beimischungen sowie die Konversion von CH_4 mittels Oxidation werden analysiert.

Als Plasma wird ein Helium Plasma mit fester CH_4 Beimischung von 0.25% und variablen Sauerstoffbeimischungen im Bereich von 0.25% bis 1% verwendet. Die Plasmaleistung wird im Bereich von 0.75 W bis 3.5 W variiert.
Die Dichten und Temperaturen der vorliegenden Spezies werden mittels Infrarotspektroskopie und theoretisch berechneten Spektren analysiert. Die bestimmten Dichten werden mit einem Globalen Modell, das die Plasmachemie beschreibt, verglichen.
Die Temperaturen der Streckschwingungen des CH_4 liegen im Bereich von 1000 K, die der Kippschwindungen stimmen mit der Rotationstemperatur überein und liegen bei 370 K, der Temperatur der Plasmakammer.
Innerhalb des Oxidationsprozesses von CH_4 wird CO als Zwischenprodukt identifiziert. Als Hauptreaktion der Oxidation von CH_4 wird die Bildung von CO_2 und H_2O bestimmt:

$$CH_4 + 2O_2 \rightarrow CO_2 + 2H_2O$$

Falls mehr als die geforderte Sauerstoffmenge bereitgestellt wird, erfolgt eine vollständige Konversion; im Falle von Beimischungen der Edukte im Verhältnis 1 : 1, erfolgt diese lediglich unvollständig. Aus dem Vergleich mit dem globalen Modell werden, von der Sauerstoffbeimischung abhänige, lineare Zusammenhänge von Plasmaleistung und Elektronendichte abgeleitet. Aus dieser Abhängigkeit lässt sich auf eine zumischungsabhängige Bildung von O^--Ionen schließen.

Die Berechnung von Absorptionsspektren von Methan stellt eine effektive Möglichkeit der Analyse von methanhaltigen Plasmen dar. Auf dieser Grundlage wurde die Plasmachemie von CH_4 O_2 Plasmen als sehr effektiv in der Bildung von CO_2 identifiziert.

Due to the high electron temperature in non-equilibrium plasmas, chemical reactions, whose activation temperatures are significantly higher than the temperature of the plasma, can take place. Due to this property of non-equilibrium plasmas, the chemical conversion of molecules can be carried out with comparably low energy expenditure.
The densities and temperatures of plasmas with different CH_4 admixtures as well as the conversion of CH_4 by oxidation are analyzed.

The plasma is a helium plasma with a fixed CH_4 admixture of 0.25% and variable oxygen admixtures ranging from 0.25% to 1%. The plasma power is varied in the range from 0.75 W to 3.5 W.
The densities and temperatures of the species are analyzed by infrared spectroscopy and theoretically calculated spectra. The determined densities are compared with a global model describing the plasma chemistry.
The temperatures of the stretching vibrations of the CH_4 are in the region of 1000 K, the temperatures of the bending vibrations correspond to the rotation temperature and are at 370 K, the temperature of the plasma chamber.
Within the oxidation process of CH_4 CO is identified as an intermediate product. As the primary reaction of the oxidation of CH_4 the formation of CO_2 and H_2O is determined:

$$CH_4 + 2O_2 \rightarrow CO_2 + 2H_2O$$

If more than the required amount of oxygen is provided, a complete conversion takes place; in case of admixtures with the ratio 1 : 1, the conversion takes place only incompletely. From the comparison of a global chemistry model, linear correlations of plasma power and electron density dependent on the oxygen admixture are derived. From this dependency it can be concluded that the amount of formed O^--ions is admixture dependent.

The calculation of absorption spectra of methane is an effective method for the analysis of methane-containing plasmas. On this basis, the plasma chemistry of CH_4 O_2 plasmas was identified as very effective in the formation of CO_2.

Contents

List of Figures

List of Tables

List of Abbreviations

EEDF	Electron energy distribution function
FTIR	Fourier-transform infrared spectroscopy
FWHM	Full width at half maximum
HiTRAN	High-resolution transmission molecular absorption
HWHM	Half width at half maximum
IEDF	Ion energy distribution function
RF	Radio Frequency
SEI	Specific energy input

1. Motivation and goals of the study

The avoidance of greenhouse gas emissions into the atmosphere is the main task in preventing an increase of the temperature of earth due to man made climate change [1]. The most present greenhouse gases are CH_4 and CO_2. Today, attempts are made to use these greenhouse gases in various industrial applications, e.g. energy storage or the production of molecules required for chemical applications.
In any of these processes a maximal energy efficiency is targeted. The energy efficiency is described by the specific energy input (SEI) per molecule. An induced dissociation process is energy efficient if the SEI is close to the necessary reaction enthalpy. An energy efficient dissociation process can take plasma by plasmolysis, the 'dissociation of a precursor gas in a plasma generated by electric fields' [2]. Plasmolysis can lead to a low SEI as the energy deposited in the plasma can be deposited in specific excitation modes. If those excitation modes are the ones causing the dissociation, high energy efficiencies can be obtained.
The conversion of CH_4 using plasmolysis is mainly done by partial or full oxidation of CH_4. Partial oxidation can either produce synthetic gas used for energy storage [3] or it can lead to methanol [4] and formaldehyd [5], both needed precursors in the chemical industry. The full oxidation of CH_4 is mainly investigated in the context of a catalyst [6, 7] with the aim to produce CO_2 and H_2O.

In order to analyse any plasma chemistry involving CH_4 a reliable and quantitative method of analysis has to be developed. The calculation of absorption spectra together with the use of Fourier-transform infrared spectroscopy (FTIR) is successfully used for the absorption spectra of CO_2 and CO [2, 8].
In order to analyse the plasma chemistry of methane containing plasmas absorption spectra of CH_4 have to be modelled. The aim of this study is to establish the calculation of absorption spectra of CH_4 as a method of analysis for methane containing plasmas. The calculated spectra shall be confirmed by experimental data and used to deduce statements about the methane containing plasmas. After applying the calculations to plasmas with methane admixtures only, the behaviour of methane in the oxidation without a catalyst shall be analysed. The aim is to gain a better understanding of the plasma chemistry of this process. This examination is done with the objective to formulated predictions for further studies of the oxidation of methane without catalysts.

In this study, the theoretical background of infrared spectroscopy and the quantum mechanical treatment of rotational and vibrational excitations is described. Based on this, the rotational and vibrational excitations of CH_4 are derived. Together with the application of different broadening mechanisms, the calculation of an absorption spectrum of CH_4 in a non-equilibrium atmospheric pressure plasma based on the high-resolution transmission molecular absorption (HiTRAN) database is outlined.
These calculated spectra are then compared to ones obtained by FTIR measurements to determine the density and temperatures of the measured plasmas. Spectra without an ignited plasma are used to calibrate the used apparatus whereas spectra with an applied generator power of 50 W are used to verify the calculated spectra in case of excited CH_4. The oxidation of CH_4 is analysed for plasmas with CH_4 admixtures of 0.25% and O_2 admixtures of 0.25%, 0.5%, and 1%. The correlation between plasma power and generator power for these plasmas is examined.
The plasma chemistry of these plasmas is analysed using the absorption spectra of CO_2, CO, and H_2O based on the work by Urbanietz et al. [2]. The trends of the densities of

the different species with respect to the plasma power are examined to deduce statements about the plasma chemistry. Based on balances of different atoms, the oxidative reaction present in the plasma is determined.

The measured densities are compared to a global model in order to verify the ascertained reaction. Based on this comparison correlations between the electron density and the plasma power are derived.

2. Theoretical background

In the following chapter, the theoretical background of the performed study is presented. After non-equilibrium plasmas are characterized, selection rules for infrared spectra of molecules are illustrated. Following that, the concept of Fourier-transform infrared spectroscopy is introduced as a method to detect those spectra.
Ensuing, the quantum mechanical treatment of rotational and vibrational excitations is described and the necessary set of equations is presented in case of CH_4. Based on the general description of the excitations, the calculation of infrared absorption spectra is described with broadening mechanisms being taken into account.

2.1 Non-equilibrium atmospheric pressure plasmas

Following Chen [9] a plasma is a 'quasineutral gas of charged and neutral particles which exhibits collective behaviour'. To quantify this definition, a plasma is defined by the following conditions:

- The term quasineutrality describes the behaviour of a gas ensemble to seem uncharged from the outside. To ensure this quasineutral behaviour, the shielding of the charges in the plasma has to be sufficient. The key parameter of shielding is the so called Debye length λ_D which is defined as:

$$\lambda_D \coloneqq \left(\frac{\varepsilon_0 k_B T_e}{n_0 e^2}\right)^{1/2} \tag{2.1}$$

  with the dielectric constant ε_0, the Boltzmann constant k_B, the electron temperature T_e, the stationary ion background density n_0, and the elemental charge e. Within one Debye length, the amplitude of an electric field, resulting from density perturbations, shrinks by a factor of e^{-1}. In order to ensure that these perturbations are damped such that they vanish for an outside observer, the dimensions of the plasma L have to exceed the Debye length:

$$L \gg \lambda_D \tag{2.2}$$

- The concept of shielding across one Debye length is only valid if enough charged particles are present in the direct surrounding of the perturbation. Based on this premise, the Debye sphere V_D is defined:

$$V_D \coloneqq \frac{4}{3}\pi\lambda_D^3 \tag{2.3}$$

  Collective behaviour of a plasma is given in case that shielding across one Debye length is a statistically reasonable assumption [9]. Therefore, the number of particles within one Debye sphere N_D has to be significantly higher than unity:

$$N_D \gg 1 \tag{2.4}$$

- Plasma oscillations are mainly driven by the movement of electrons due to their low mass in comparison to the molecules or atoms. To quantify the movement of the electrons, the plasma frequency ω_{pe} is defined as:

$$\omega_{pe} \coloneqq \left(\frac{n_e e^2}{\varepsilon_0 m_e}\right)^{1/2} \tag{2.5}$$

with the electron density n_e and the electron mass m_e. In order to distinguish between plasma and gas, the particle interaction mechanism that dominates the ensemble, is of importance. In case of a plasma, the electromagnetic force is the dominant mechanism, whereas hydrodynamic forces are prevailing in a gas. In order to decide which of the mechanisms is dominant the product of plasma frequency ω_{pe} and time between collisions with neutrals τ is examined. With the claim that the product of the two parameters is greater than unity, it is ensured that electromagnetic interactions are the dominant mechanism of particle interaction. That leads to:

$$\omega_{pe}\tau \gg 1 \tag{2.6}$$

Due to the low ionisation degree of non-equilibrium plasmas, this condition does not hold true for the plasmas used in this study.

2.2 Selection rules for electric dipole transitions

Besides being in their energetic ground state molecules can also be present in energetically excited states. A transition between two different energetic states often takes place via the emission or absorption of a photon. For these transitions restrictive selection rules are present. In the following, the selection rules of photons in the infrared region originating from rotational or vibrational excitations are described.
The main sources of infrared light within the spectra of molecules are rotational and vibrational excitations. As dipole radiation is the dominant channel of emission for these kinds of relaxation, it is sufficient to only take this kind of radiation into account. The dipole moment of a molecule μ_{tot} can be separated into an electronic part μ_e, induced by the electrons of the molecule and a nuclear part μ_n, resulting from the charges of the nuclei:

$$\mu_{tot} = \mu_e + \mu_n \tag{2.7}$$

Transitions resulting from the electronic part of the dipole moment refer to transitions between two different electronic states which are described by the Franck-Condon-Principle. As electric transitions are not object of analysis and it is assumed that this part of the dipole moment does not affect vibrational and rotational excitations, this segment of the dipole moment is neglected.
The nuclear part of the dipole moment of a molecule can be approximated using [10]:

$$\mu_n = \mu_0 + \frac{d\mu}{dQ}\Delta Q \tag{2.8}$$

with the permanent dipole moment μ_0, the coordinate Q describing the position of the nuclei, and the change of dipole moment with respect to Q, $\frac{d\mu}{dQ}$.
The rotational spectrum of a molecule can only be infrared active if the molecule has a permanent dipole moment [10]. Due to symmetry reasons, a permanent dipole moment can only be present along an axis of symmetry. The main implication is that molecules with more than one symmetry axis can not have an infrared active rotational spectrum [11].
In case of a vibrational excitation, thus, a change in the coordinate Q with respect to time, the dipole moment varies with the frequency of oscillation, assuming $\frac{d\mu}{dQ}$ is non-zero [10]. This change of dipole moment is necessary for the molecule to be able to interact with any kind of dipole radiation.
Vibrational selection rules are only present if a molecule possesses elements of symmetry [11]. In case of an existing symmetry two selection rules determine whether a vibrational excitation of a molecule is infrared active or not. In case that these two rules allow infrared

active transitions, two additional selection rules give further restrictions to the transitions themselves.
In order to have an infrared active vibrational mode, the product of the wave functions of the upper state ψ_u of the transition and the lower state ψ_l of the transition with one of the axes of the dipole moment μ_i has to be totally symmetric [12]:

$$\psi_l \psi_u^* \mu_i \quad i = x, y, z \tag{2.9}$$

with the complex conjugate of the wave function of the upper state ψ_u^*. For transitions involving the ground state only the symmetry of the upper state is taken into account as the ground state itself is totally symmetric.
The second selection rule a molecule has to fulfil to have infrared active vibrational modes results from a quantum mechanical treatment. It demands that a vibrational transition is only allowed if the vibrational mode has the same symmetry as the dipole moment of the molecule [10].
In case that infrared active transitions are allowed the following two selection rules give further restrictions for the transitions themselves:

$$\sum |\Delta\nu_i| \geq 1 \tag{2.10}$$

$$g \leftrightarrow u \tag{2.11}$$

with 2.10 referring to the change of at least one vibrational quantum number ν_i *and 2.11 only allowing transitions between states of different symmetries g and u, referring to symmetric and antisymmetric states, respectively.* Selection rule 2.10 allows transitions of almost arbitrary chosen ν_i but it has to be noted that transitions of higher $\sum |\Delta\nu_i|$ are weaker than the ones of $\sum |\Delta\nu_i| = 1$.

2.3 Absorption measurements

Light travelling through whatever medium loses intensity due to absorption or scattering by the particles of the medium. The absorption rate of light in a gaseous medium can be characterized by the following differential equation:

$$\frac{\partial N_n}{\partial t} = -N_n B_{nm} w_\gamma \tag{2.12}$$

with m and n referring to indices of different energy levels, the number of particles in the lower energetic state N_n*, the Einstein coefficient of induced absorption* B_{nm} *between the states m and n, and the spectral radiation density* w_γ*.* The Einstein coefficients of induced absorption B_{nm} and spontaneous emission A_{nm} are proportional to each other which allows to identify a measured absorption with the Einstein coefficient of emission. If one solves the differential equation and identifies the number of particles in the lower state with the remaining intensity of light, the Lambert-Beer law is obtained:

$$I = I_0 e^{-\alpha d} \tag{2.13}$$

with the initial intensity I_0*, the length of the optical path d, the absorption coefficient* α*, and the remaining intensity I.* The absorption coefficient is directly related to the strength of an emission line S_{nm} and the density of the species n like:

$$\alpha_{nm} = S_{nm} n f \tag{2.14}$$

with the normalized line profile f and $S_{nm} \propto B_{nm}$*.* The Lambert-Beer law is used in section 2.6 together with the behaviour of the absorption coefficient to calculate infrared absorption spectra.

2.4 Fourier-transform infrared spectroscopy

Measurements of absorption spectra can be executed using different methods. A method in which a wide spectral range can be covered is the-Fourier transform infrared spectroscopy (FTIR). In an FTIR setup an interferometer is used to obtain an absorption spectrum dependent on a spatial coordinate. Using Fourier transformation this spatial coordinate can be transformed into a wavenumber coordinate which is more suited for later analysis. In general, the setup is based on a Michelson interferometer with one of the mirrors being movable. A sketch of the interferometer is displayed in figure 2.1.

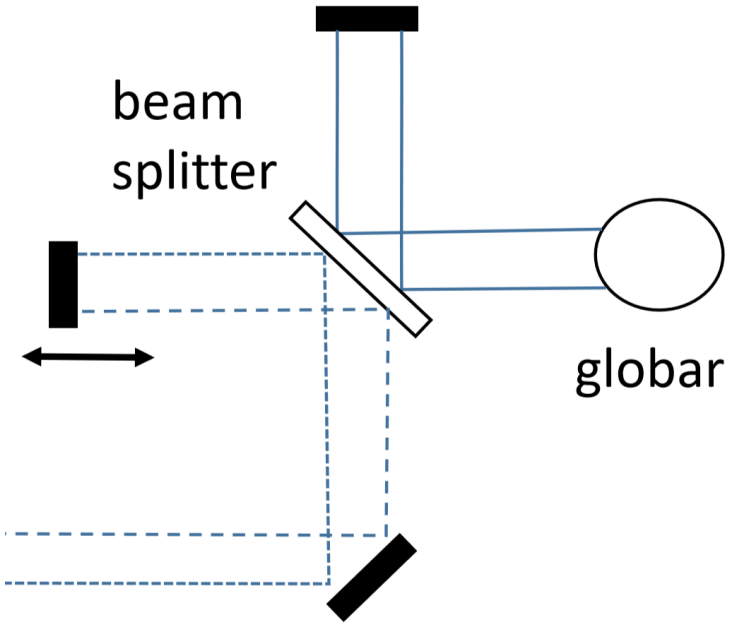

Figure 2.1: Sketch of the FTIR spectrometer, adapted from [2].

The globar emits light which incidents upon the beam splitter. From the beam splitter the light is partly transmitted and partly reflected, resulting in two light beams falling onto the mirrors which are placed perpendicular to each other. The mirrors reflect the light and using the beam splitter the two beams are merged and guided outside the FTIR. The light intensity of the merged beam is dependent on the phasing of the two beams due to interference. The merged beam can then be used to analyse a gaseous medium by detecting its light intensity after the transit.
As one of the mirrors can be moved along the beam path the phasing between the two light beams changes. The movement of the mirrors is done in steps of length Δx, resulting in a difference of path length $\Delta L = 2n\Delta x$, $n \in \mathbb{N}_0$. Based on the setup, the criterium for constructive interference is given by:

$$\Delta L = k\lambda \tag{2.15}$$

with the difference in path length ΔL, $k \in \mathbb{Z}$, *and the wave length* λ. The spatial information of the movable mirror is obtained by analysing the interference of a laser of known wavelength. This laser is pointed directly onto the movable mirror and its interference pattern is analysed, yielding spatial information about its position.
From the measurements of the position of the mirror, as well as the detected light intensity a spectrum depending on the wavenumber ν can be calculated using Fourier transformation:

$$I(\nu) = \sum_{k=0}^{N-1} I_0 \exp\left(-2\pi i k n/N\right) \tag{2.16}$$

with the total number of mirror steps N, the initial intensity I_0, and the condition for constructive interference $k \in \mathbb{Z}$. Due to the transform, the resolution in the wavenumber space is reciprocal related to the number of mirror steps and the length of these steps like:

$$\Delta\nu = \frac{1}{\Delta x N} \tag{2.17}$$

2.5 Excitation of molecules inside a plasma

In the following section, the theoretical background for rotational and vibrational excitations is illustrated. Furthermore, the necessary formulas and parameters in case of CH_4 are derived to provide these information for a theoretically calculated spectrum of CH_4 which is explained in section 2.6.

2.5.1 Excitation modes

The kinetic energy of a particle can be described by its velocity with respect of three chosen spatial directions [10]:

$$E_i\left(\dot{x}_i, \dot{y}_i, \dot{z}_i\right) = \frac{1}{2} m_i \left(\dot{x_i}^2 + \dot{y_i}^2 + \dot{z_i}^2\right) \tag{2.18}$$

with the mass of the particle m_i and the velocities $\dot{x}_i$, $\dot{y}_i$, and $\dot{z}_i$ around the three spatial directions x, y, and z. Due to the three different spatial dimensions any given particle has three degrees of spatial freedom. Thus, a system of N independent particles has $3N$ degrees of freedom in total with the energy of each particle being individually described by equation 2.18. If the particles form a rigid system, the number of translational degrees of freedom shrinks. The only translation present is the one of the center of mass moving relative to the chosen coordinates. Therefore, translation only takes up three degrees of freedom with the other $3N - 3$ being available for other excitations.

In general, the energy of a molecule can be approximated by the energy contributions of its different kinds of motion [13]:

$$E = E^T + E^R + E^V + E^E \tag{2.19}$$

with the translational energy E^T, the rotational energy E^R, the vibrational energy E^V, and the electronic energy E^E. In reality, the electric energy is not a motion but can be treated like one [13]. The separation of the electronic and the vibrational motion is only valid if the electrons are in their ground state [13]. This is valid for the observed kind of plasmas due to their low ionisation degree. In the following, only vibrational and rotational excitations are considered. Translational energy is covered by the Doppler shift described in section 2.7.2 and the electrons are assumed to be in their ground state.

As symmetry is a key parameter for the vibrational and rotational excitations of a molecule, molecules are sorted in so called point groups [14]. In the following, only the point group of CH_4 will be further investigated.

Rotational excitation mode

The rotational excitation of a molecule is present in the form of rotations along three spatial axes around its centre of mass. In case of molecules of simple geometry, e.g. CO_2, the number of axes can be lower. The number of degrees of freedom being occupied by rotation R is equal to the number of rotational axes.

In a quantum mechanical treatment of rotations, the different rotational levels are parametrized by the quantum number of total angular momentum j. Based on this quantum number the rotational energy levels of a molecule are calculated using up to three constants $B_{[\nu]}$, $D_{[\nu]}$, and $H_{[\nu]}$. These constants are defined for a rotation around a certain chosen axis and are mainly dependent on the moment of inertia along this axis. The constant $B_{[\nu]}$ is the 'rotational constant' [12] describing the genuine energy levels. The constant $D_{[\nu]}$ is used to compensate the 'influence of centrifugal stretching' [11] and is small in comparison to $B_{[\nu]}$. $H_{[\nu]}$ provides further corrections but is typically negligibly. The subscript ν refers to the fact that those constants are in general dependent on the vibrational state ν if both, rotational and vibrational excitations, are present [12]. This dependency results from contributions of vibrational excitations to the total energy of the state. As those contributions are rather small in comparison to the parts resulting from the moments of inertia they can be neglected in cases of low vibrational excitations. The ones covered in this study are sufficiently low to fulfil this condition.
In the following, the occupancy of the different rotational levels is assumed to be thermalized since the Maxwell distribution describing thermal equilibrium is the simplest assumption. The Maxwell distribution is described in section 2.5.3.

Vibrational excitation modes

The remaining unoccupied $3N - 3 - R$ degrees of freedom determine an upper limit to the number of normal vibrations that can occur within a molecule. A normal vibration can be defined as 'a vibrational state in which each atom carries out a simple harmonic motion about its equilibrium position' [10]. For each degree of freedom a normal vibration exists. All normal vibrations with the same frequency of oscillation belong to the same vibrational mode, contributing to the degeneracy of the specific mode d_i.
Vibrational excitations can be approached assuming the harmonic oscillator potential. Due to these considerations the degeneracy of a vibrational state with degeneracy d_i of its mode is given by [15]:

$$g(\nu_i) = \begin{cases} d_i = 1 & 1 \\ d_i = 2 & \nu_i + 1 \\ d_i = 3 & \frac{(\nu_i+1)(\nu_i+2)}{2} \end{cases} \tag{2.20}$$

with the vibrational quantum number ν_i and the degeneracy of the state $g(\nu_i)$.
The energy of a single vibrational states is also known from the assumption of a harmonic oscillator potential. The total energy deposited in the several vibrational excitations corresponds to the sum of the energies of the single states [13]:

$$E_{vib}\left(\nu_1, ..., \nu_n\right) = \sum_{i=1}^{n} E_{\nu_i} = \sum_{i=1}^{n} h f_i \left(\nu_i + d_i/2\right) \tag{2.21}$$

with the maximum number of vibrational modes n, the vibrational frequency f_i, and Planck's constant h.
Equation 2.21 only holds true in case of pure vibrational excitations. The molecule is distorted by centrifugal forces in case of additional rotational excitations being present. Due to this distortion the amplitudes of the vibrational modes are changed, yielding a shift of the energy levels of each single state. This problem is avoided using the HiTRAN database which provides distortion constants for the various vibrational modes of a molecule [16]. The implementation of these into the calculation of a spectrum is illustrated in subsection 2.6.2.
Similar to the rotational case a Maxwell distribution is assumed since the vibrational degrees of freedom are estimated to be thermalized. As the different vibrational modes are independent on each other, each of them is described by its own distribution function with individual parameters.

2.5.2 Spherical top molecules

A spherical top molecule 'has two or more three-fold or higher fold axes' [11]. An n-fold axis is defined as an axis within the molecule along which it can be rotated by $360/n$ degrees without changing its moment of inertia. Due to these symmetries all moments of inertia along the chosen axes in a spherical top molecule are equal : $I_A = I_B = I_C$.
The spherical top present in the study is CH_4. It belongs to the point group T_d which is a sub group of the spherical top molecules. The T_d point group has 'three mutually perpendicular two-fold axes and four three-fold axes as well as planes of symmetry, σ_d, through each pair of three-fold axes' [14]. Those symmetry properties lead to a molecule of a tetrahedral shape. Due to this symmetry CH_4 does not have an infrared active rotational spectrum as described in section 2.2.

Rotational energy levels of spherical top molecules

As already mentioned in section 2.5.1, the rotational spectra of most molecules can be calculated from two rotational constants which are mainly dependent on the moments of inertia within the molecule. Due to the three moments of inertia being equal in case of CH_4 the influence of centrifugal stretching within spherical tops is neglectable. This leads to a simple formula for the rotational energies E_{rot} [11]:

$$E_{rot}(j) = Bj(j+1) \tag{2.22}$$

with the rotational constant B. The subscript of the rotational constant is neglected as the constant is approximated to be independent on the vibrational excitation. The specified energy levels match those from a simple quantum mechanical rotator.

Rotational degeneracy of spherical top molecules

The degeneracy of a rotational excitation in case of a spherical top molecule is exclusively dependent on the quantum number j. For all rotational excitations a factor of $2j+1$, the so called space degeneracy, is existent in the degeneracy of a state of quantum number j. This factor originates from the fact that the vector $\vec{J}$ can have any orientation with respect to an arbitrary chosen axis within the molecule [11].
Even though all moments of inertia within a tetrahedral molecule are equal three types of rotational levels called A, E, and F exist [11]. These occur due to the non-zero spin of the hydrogen atoms and the resulting statistics. Depending on the spin orientation of the single atoms three different total spin configurations namely, $T = 2$, $T = 0$, and $T = 1$ can be formed. Those are referred to as nuclear quintet, nuclear singlet and nuclear triplet, respectively. Each of these states has its own degeneracy but as all belong to the same rotational state the degeneracy of the state is given by their sum. Rules to determine the degeneracies in particular can be calculated using group theory which was done by Wilson [17]. The related results can be found in table A1.1 in appendix A1.

Vibrational degeneracy of spherical top molecules

In section 2.5.1 it was mentioned that the total energy of the vibrational excitations can be calculated from equation 2.21 but is taken from the HiTRAN database. The missing parameter in order to be able to describe the vibrational excitations of CH_4 mathematically is the degeneracy of the different vibrational excitations. As mentioned in section 2.5.1 the degeneracies can be calculated on the base of a harmonic oscillator potential with the related degeneracies given by equation 2.20. To use this equation the degeneracies of the different vibrational modes need to be known. The normal vibrations of CH_4 are displayed in figure 2.2.

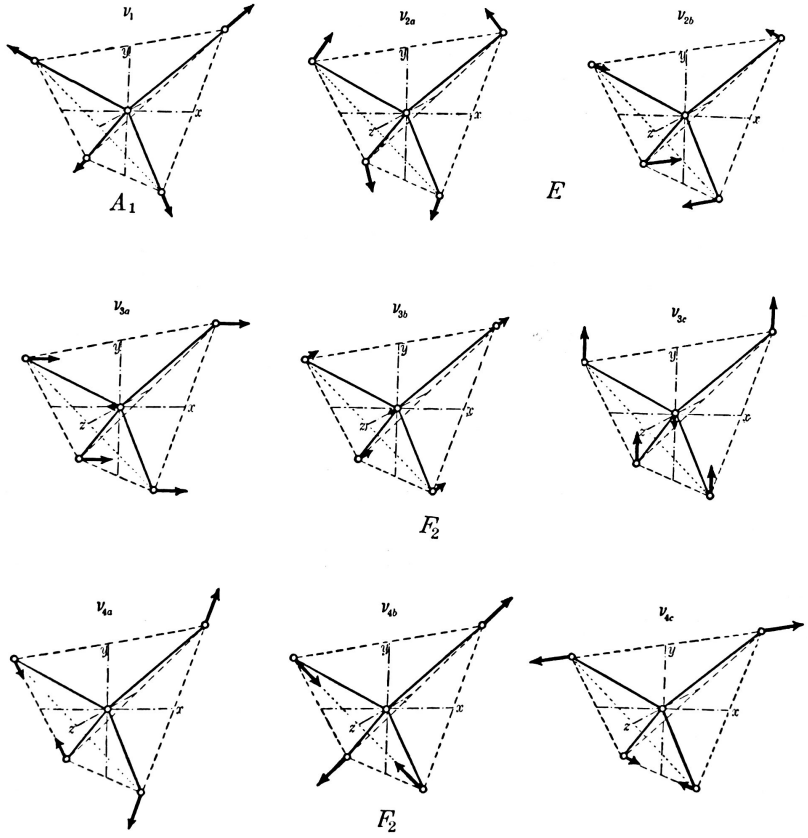

Figure 2.2: Normal modes of the vibrational excitations of CH_4, grouped by their excitation modes [11].

In total, four different vibrational modes with unique vibrational frequencies are present, namely a symmetric stretching mode ν_1 with a degeneracy of one, an infrared inactive bend ν_2 with a degeneracy of two, an asymmetric stretching mode ν_3 with a degeneracy of three, and an infrared active bend ν_4 with a degeneracy of three as well [18]. The frequencies referring to the normal vibrations can be found in table A1.2 in appendix A1. The labels A_1, E, and F_2 refer to different vibrational states, similar to the rotational states given in 2.5.2. These different vibrational states again result from the statistics induced by the spin of the hydrogen atoms. Based on equation 2.20 the degeneracies of the different vibrational excitations of CH_4 $g_{\nu_i}(\nu_i, k)$ are:

$$g_{\nu_i}(\nu_{i,k}) = \begin{cases} g_{\nu_1} = 1 \\ g_{\nu_2} = \nu_{i,k} + 1 \\ g_{\nu_3} = \frac{(\nu_{i,k}+1)(\nu_{i,k}+2)}{2} \\ g_{\nu_4} = \frac{(\nu_{i,k}+1)(\nu_{i,k}+2)}{2} \end{cases} \tag{2.23}$$

with the vibrational mode ν_i and the vibrational quantum number of this mode $\nu_{i,k}$.

2.5.3 Distribution functions

Even though the ions in non-equilibrium plasma are not thermalized it is assumed that the rotational and vibrational degrees of freedom of the observed species are thermalized. In general, any thermalized species is described by a Maxwell distribution.

Maxwell distribution

A Maxwell distribution describes the probability distribution of a system with respect to the global parameter temperature T and the free parameter energy E:

$$p = A \times g(E) \exp\left(-\frac{hc}{k_B}\frac{E}{T}\right) \tag{2.24}$$

with a normalization factor A, the speed of light c, Planck's constant h, Boltzmann's constant k_B, and the degeneracy $g(E)$ at the chosen energy. The normalization constant is obtained by integrating over the energy and by demanding that the total probability has to be equal to unity. As the different excitation modes are assumed to be independent on another the occupation of states of each of them follows an individual Maxwell distribution with unique temperatures.

Partition functions

In a quantum mechanical treatment, only discreet energy levels are allowed. Therefore, the probability distribution is no longer continuous but has the shape of different weighted δ-distributions. The normalization factor transforms into a sum as the normalization is nonetheless given by an integral, yielding the so called partition function $Q(T)$:

$$Q(T) = \sum_{i=0}^{i_{max}} p\left(E_i\right) \tag{2.25}$$

with i_{max} being an upper level of potentially excited states and the probability of occupancy of a state in the Maxwell distribution $p(E_i)$. An upper limit for the excited states is chosen as the probability of occupation for levels of high E is low in case of a low temperature. In case of molecular excitations in non-equilibrium plasmas i_{max} is in the order of 100.

2.6 Calculation of line strengths using the HiTRAN database

In order to be able to calculate absorption spectra molecular constants as well as transition information of the examined molecule have to be known. The HiTRAN database provides these information for various molecules. The information about the different transition lines is stored in a standardized, 160 character long format which is explained in table A1.3 in appendix A1 [19]. In this study, the information provided by the HiTRAN database is used to calculate absorption spectra of CH_4, CO_2, CO, and H_2O. The molecular constants referring to these molecules are displayed in table A1.2 in appendix A1.
In order to calculate the absorption of a certain species the database can be used in two different manners, namely rescaling of given line strengths using temperatures or calculating the line intensity using the Einstein coefficients.
A simplification of the first mentioned method is used in this study to determine the H_2O density. The line strengths at 300 K are read out of HiTRAN and rescaled using the density. This method yields densities with rather large errors due to the missing adjustment of temperatures and was used due to the sophisticated quantum mechanical statistics of H_2O.
The latter method which yields more precise results is used for the species CH_4, CO_2, and CO as their quantum mechanical statistics are suited for this methode. The statistics of CH_4 are described in section 2.5.2 and the statistics of the other two species can be found in the books [12] respectively [14] by Herzberg.

2.6.1 Calculation of the rotational distribution function

The energy levels of the rotational excitations of CH_4 are described by equation 2.22, the related degeneracies are calculated using table A1.1 and the ones of CO and CO_2 can be found in the earlier mentioned books by Herzberg. With the rotational energies and the related degeneracies the probability distributions of the rotational levels can be calculated. A Maxwell distribution as described in equation 2.24 was assumed with a partition function $Q_{rot}(T)$ as the element of normalization:

$$p = \frac{g_{rot,j}}{Q_{rot}(T)} \exp\left(-\frac{hc}{k_B}\frac{E_{rot,j}}{T_{rot}}\right) \tag{2.26}$$

with the statistical weight of the rotational state $g_{rot,j}$, the energy of the rotational state $E_{rot,j}$, and the rotational temperature T_{rot}. A partition function based on equation 2.25 is used. To calculate the initial probabilities $Q_{rot}(T)$ is set to unity and adapted afterwards. The upper limit i_{max} is chosen for every molecule independently, based on the data provided in table A1.2 in appendix A1.

2.6.2 Calculation of the vibrational distribution function

In section 2.5.1 it was described that equation 2.21 is not valid in case of a rotationally excited molecule due to centrifugal distortion. In order to bypass this issue the HiTRAN database provides constants for centrifugal distortion $\omega_e x_{e,i}$ of the different vibrational modes. These can be used to directly calculate the probability of occupancy of a certain state. The formula that describes the occupancy of the vibrational state i, is given by:

$$p_{vib,i} = \frac{g_{vib,i}}{Q_{vib,i}} \exp\left(-\frac{hc}{k_B}\left(\nu_i \frac{G_i}{T_{vib,i}} - \nu_i\left(\nu_i - 1\right)\frac{\omega_e x_{e,i}}{T_{rot}}\right)\right) \tag{2.27}$$

with the statistical weight of the state $g_{vib,i}$, the partition function $Q_{vib,i}$, the vibrational quantum number of the state ν_i, the energy of the state in wavenumbers G_i, and the rotational temperature T_{rot}. The necessary statistical weights in case of methane are calculated using equation 2.23. The vibrational degeneracies of the other two species are described by the harmonic oscillator potential as well and the degeneracies are given by equation 2.20 based on the degeneracies of the vibrational modes. The constants of centrifugal distortion are provided in table A1.2 in appendix A1.
Within the calculation of the probability of a certain state, $T_{vib,i}$ is a variable parameter, the value of T_{rot} was fixed in the rotational distribution function. The partition function is again calculated using 2.25 after calculating the single probabilities assuming $Q = 1$.

2.6.3 Calculation of the line strength of absorption

The probability for a particular state to be occupied results from the product of the probabilities of its vibrational and rotational states to be occupied:

$$p_{total,j,\nu_1,\ldots,\nu_l} = p_{rot,j} \times \prod_{l=1}^{l_{max}} p_{vib,l} \tag{2.28}$$

with the probability of the rotational state of quantum number j, $p_{rot,j}$, the probability of the vibrational mode l, $p_{vib,l}$, and the number of vibrational modes l_{max}. Using the probabilities of two different states m and n the line strength S_k of a certain transition can be calculated using the following formula:

$$S_k = p_{isotope}\frac{g_{rot,u}A_{n,m}}{8\pi\nu_k^2}\left(\frac{p_{total,n}}{g_{rot,n}g_{vib,n}} - \frac{p_{total,m}}{g_{rot,m}g_{vib,m}}\right) \tag{2.29}$$

with the isotopical abundance $p_{isotope}$, the Einstein coefficient $A_{n,m}$ for a transition between the states m and n, and the wavenumber of the transition ν_k. The isotopical abundances of the different molecules are shown in table A1.2 in appendix A1. The given abundances indicate that it is reasonable to solely include the most present isotopologue of each species into the calculations.

2.6.4 Modelling of the resulting spectrum

Using the Lambert-Beer law given by equation 2.13 the transmission of a plasma at wavenumber k can be expressed by:

$$T(k) = \frac{I}{I_0} = \exp\left[-\alpha(k)d\right] \tag{2.30}$$

with the initial and resulting intensities I_0 and I, respectively, the absorption coefficient $\alpha(k)$ and the length of the optical path d. The absorption coefficient is described by equation 2.14 and is directly related to the line strength described by equation 2.29. The dependency on the indexes m and n is replaced by the parameter k as only the energy of the transition is of importance.
This formula describes the transmission at the wavenumber of the absorption line. In order to be compare a calculated spectrum to a measured one different broadening mechanisms have to be applied.

2.7 Line broadening

In general, three different broadening mechanisms have to be considered:
Pressure broadening, Doppler broadening, and instrumental broadening
Whereas the first two mechanisms are plasma specific the latter one is dependent on the experimental setup in use. In order to describe the broadening mechanisms caused by the plasma, Gaussian and Lorentz distributions have to be introduced.

Gaussian distribution

A Gaussian distribution is used in order to describe a normal distribution of standard deviation σ around a mean value μ of the free parameter ν:

$$G(\nu) = \frac{1}{\sqrt{2\pi\sigma^2}} \exp\left(-\frac{(\nu-\mu)^2}{2\sigma^2}\right) \tag{2.31}$$

In the application, a Gaussian distribution is used in the context of Doppler broadening in subsection 2.7.2 as well as in the instrumental broadening in section 2.7.3.

Lorentz distribution

A Lorentz distribution is used to describe the strength of a resonance at wavenumber ν around the resonance value ν_0 with the width γ:

$$L(\nu) = \frac{1}{(\nu^2-\nu_0^2)^2 + \gamma^2\nu_0^2} \tag{2.32}$$

In this context a Lorentz profile occurs in the context of pressure broadening in section 2.7.1.

2.7.1 Pressure broadening

Pressure broadening occurs due to the collision of an excited particle with another particle during its emission process. The emission process of the excited particle is interrupted, resulting in the total time of the emission process being shortened. The half width at half maximum (HWHM) of this broadening mechanism is given by:

$$\gamma(p,T) = \left(\frac{T_{ref}}{T}\right)^{n_{air}} (\gamma_{air}(p - p_{self}) + \gamma_{self} p_{self}) \tag{2.33}$$

with the reference temperature T_{ref}, the temperature T, the pressure p, the pressure of the species p_{self}, and the broadening parameters γ_{air} and γ_{self} with the latter two provided by HiTRAN. As the duration of the emission process is shortened, the emission line is shifted towards higher wavenumbers like:

$$\nu_{ij}^{*} = \nu_{ij} + \delta_{shift} p \tag{2.34}$$

with the initial wavenumber ν_{ij} and the shift coefficient δ_{shift}. To simplify calculations no distinction between the different species is made and self-broadening is assumed to be the dominant mechanism. The reference parameters p_{self} and T_{ref} are set to 1 bar and 296 K, respectively by the HiTRAN database. The temperature of the plasmas is chosen to be the mean of the temperatures in the underlying set of temperatures used for the calculated spectrum.
The resulting broadened spectrum follows the shape of a Lorentzian profile:

$$f(\nu) = \frac{1}{2\pi} \frac{\gamma}{(\nu - \nu_0)^2 + \left(\frac{1}{\gamma}\right)^2} \tag{2.35}$$

2.7.2 Doppler broadening

As mentioned in section 2.5.1 one of the excitation modes of molecules is translational movement. This motion is present in the movement of single molecules with respect to fixed coordinates describing the plasma and is based on the temperature of the plasma. As the molecules move the wavelength of light emitted by them is changed due to a Doppler shift. As the velocities follow a normal distributed with respect to all spatial directions, the broadening of the absorption lines follows a Gaussian distribution with a HWHM of:

$$\alpha_D = \frac{\nu_{ij}}{c} \sqrt{\frac{2 N_A k_B T \ln(2)}{M}} \tag{2.36}$$

with the molar mass M and the Avogadro constant N_A.

Convolution of Gaussian and Lorentzian

As both broadening mechanism occur parallel both have to be applied onto the calculated spectrum at the same time. A parallel application is done by calculating the convolution of the two broadening mechanisms which results in a Voigt profile:

$$f(\nu) = (G * L)(\nu) = \int_{-\infty}^{\infty} G(\tau) L(\nu - \tau) d\tau \tag{2.37}$$

with the Gaussian profile $G(\nu)$ and the Lorentz profile $L(\nu)$.
A Voigt profile only has to be used if the two broadening mechanisms are of similar size. In the analysed plasmas the HWHM of the Lorentzian profile is much bigger than the one of the Gaussian profile. This is caused by the high pressure and the low temperature of

the system. Therefore, it is sufficient to only take pressure broadening into account.
The profile of the pressure broadening is applied to the line strengths calculated using equation 2.29, yielding a Lorentzian shaped realm of line strengths around the initial absorption line. Using these values the absorption coefficient at the given wavenumber can be calculated using equation 2.14. The absorption spectrum can then be calculated using the Lambert-Beer law described in equation 2.13.
From these calculations a spectrum is obtained which is broadened by the dominant broadening mechanism within the plasma.

2.7.3 Instrumental broadening

The calculated spectrum corresponds to the one emitted by the plasma. Due to the use of detectors, an additional broadening mechanism, the instrumental broadening, has to be taken into account.
The instrumental broadening is covered by the application of a Gaussian distribution for each of the data points present in the calculated spectrum. The measured absorption at wave vector k is calculated from the absorption calculated by the Lambert Beer law $T(k')$ like:

$$T_{meas}(k) = \frac{1}{A} \int_{-\infty}^{\infty} T(k') \exp\left(-\frac{(k-k')^2}{\Delta k^2}\right) dk' \tag{2.38}$$

with the norm A and the chosen steps in wave vector space Δk.
Performing these calculation over the whole wavenumber space, yields an calculated absorption spectrum. In order to fasten these calculations the Gaussian is calculated based on a close region around the chosen wavenumber, determined by the selected intervals in the wave vector space.

Parameters determined by the comparison

The free parameters plugged into the calculations are the density of a species as well as the rotational and vibrational temperatures of it. From the comparison of a measured spectrum with a calculated one, it is therefore possible to determine values for these parameters by finding the best match of the two spectra. How this comparison is done in particular is described in section 3.5.

3. Experimental setup

3.1 Motivation for the use of a non-equilibrium atmospheric pressure plasma

Due to atmospheric pressure plasmas having experimental advantages over low-pressure plasmas, a plasma fitting those requirements is used in this study. As the pressure inside and outside the plasma chamber is equal, no vacuum pumps are needed to perform the measurements. Due to the high flow of cold gas and the consequential short residence time inside the chamber the ions can not form a thermal equilibrium. Emerging from this, most of the dissipated energy is used to excite electrons, resulting in hot electrons (3 eV) and an ion temperature around room temperature (25 meV). Therefore, a non-equilibrium within the ion energy distribution function (IEDF) is present, while the electron energy distribution function (EEDF) is thermalized.
In the study the plasma chemistry of He plasmas with different admixtures of CH_4 and O_2 is examined. Helium is used as a buffer gas as it provides a favourable environment for the plasma chemistry of the admixtures. Furthermore, He plasmas can be operated at rather low generator powers in a RF discharge. In order to preserve a stable plasma and to have a reasonable amount of the examined species in the plasma the inflow of these is chosen to be in the order of 1% of the He inflow. Due to helium being a noble gas no reactions of it with the admixed gases are expected. Furthermore, helium plays a crucial role in the excitation of the other species as excited helium molecules (He^*) can excite some of the excitation modes of the admixed species.
Based on the densities of the different species present in the plasma a partial pressure can be assigned to each species. The partial pressure is the pressure that would be present in the plasma if only the chosen species contributed to the total pressure. The partial pressure is directly related to the density of a species through the temperature of the plasma using the general gas equation.

3.2 Setup of the plasma chamber

A RF-plasma discharge between two plane electrodes is used as a plasma source. Sketches from the side of the plasma chamber and its front are presented in figure 3.1.
The frame of the setup consists of an aluminium housing and contains recesses for the electrodes as well as windows to execute spectroscopic measurements. As electrodes two 13 mm × 26 mm large and 0.5 mm thick copper electrodes are used. These are mounted parallel inside the aluminium housing and define the plasma volume. In order to prevent a current from flowing between the electrodes each of them is covered with a 1 mm thick glass plate. To prevent the aluminium housing from building up a potential a macor insulator is mounted on the back side of the electrodes. From the size of the chosen electrodes and the distance between the two glass plates a plasma volume of the size of 1 mm × 13 mm × 26 mm is defined. The total gas channel, enclosed by the isolating glass plates, has dimensions of 1 mm × 13 mm × 56 mm in height, width, and length, respectively.
The perpendicular walls of the plasma chamber consist of KBr windows due to the possibility to analyse the confined plasma using infrared light. The axis of gas flow is defined as the x-axis in figure 3.1. The gas enters the chamber through the gas inlet on the right hand side. The beginning of the gas channel is set to $x = 0$ mm. As the room between the electrodes begins 14 mm further in the x-direction it is assured that the incoming gas

flow can be assumed to be homogeneous and laminar. Due to the symmetry of the plasma chamber the gas outlet is located behind the end of the gas channel at around $x = 54\,\text{mm}$. The gas flow is controlled by one mass flow controller for each species.
The plasma is powered by a RF power supply with a frequency of 13.56 MHz which is applied to the two copper electrodes. The used power supply is operated in power mode, thus a constant power is applied to the two electrodes. A VI probe is used to determine the plasma power. This probe determines the current and voltage, as well as their phase shift, by measuring the related RF line.

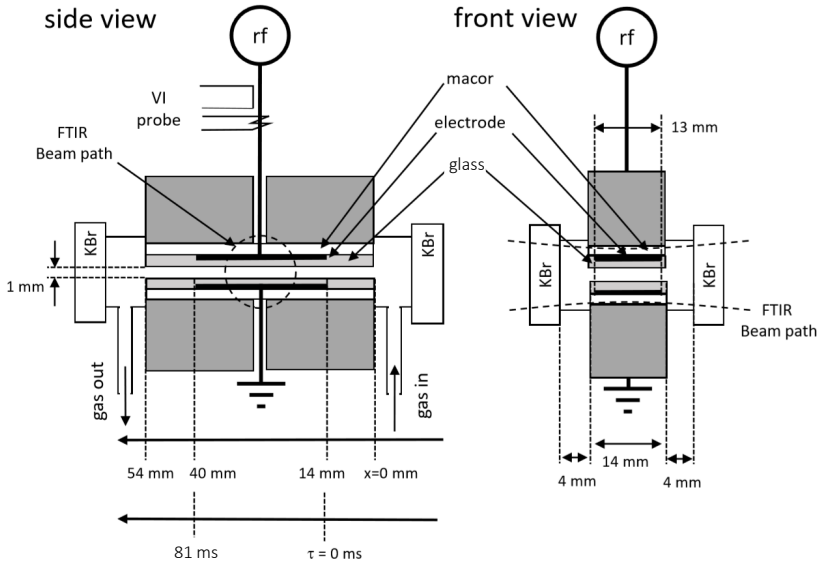

Figure 3.1: Schematic layout of the plasma chamber, adapted from [2].

3.3 Setup of the FTIR beam path

The optical analysis is performed using a Bruker IFS 66 FTIR with detection of the signal by an external MCT detector. A scheme of the setup is presented in figure 3.2. The dashed box labelled 'FTIR' refers to the setup of the Bruker IFS 66 while the dashed box labelled 'Sample compartment', describes the external beam path within the experimental setup. The FTIR works as described in section 2.3.

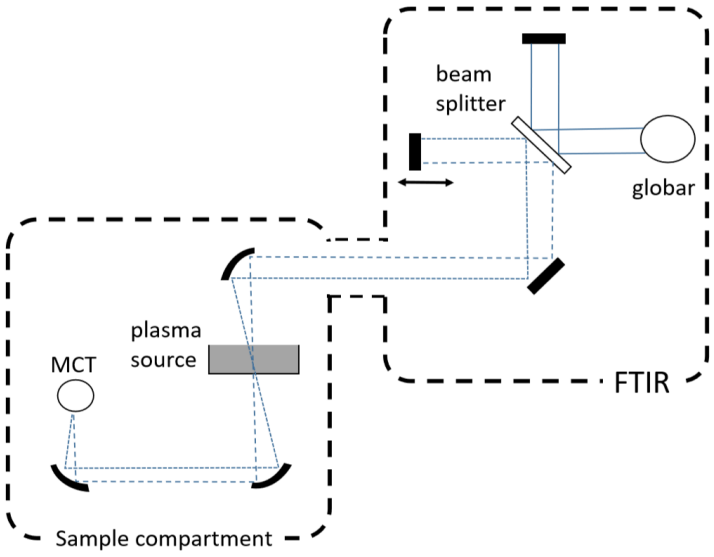

Figure 3.2: Sketch of the experimental beam path used in the FTIR measurements [2].

A mirror is used to focus the parallel light, exciting the interferometer, onto a focus point within the plasma volume (compare figure 3.1). This ensures that the whole light exiting the FTIR is used. The partly absorbed light widens up after its transit through the gas chamber and a second mirror is brought into the beam path in order to parallelize the beam again. The parallelized beam falls onto a third mirror whose focus point is located at the MCT detector. The signals of detector and FTIR are gathered by one computer and evaluated following equation 2.16.
The resulting spectrum is revised using an earlier determined background spectrum in order to ensure that all observed effects are invariably caused by the plasma. In order to reduce contributions of gases contained in the atmosphere of the room, the sample compartment is closed and constantly rinsed by a flow of 20 slm of nitrogen. As nitrogen is infrared inactive it does not occur in the measured spectra.

3.4 Performed measurements

At first, measurements with various admixtures of CH_4 in plasmas of different He flows were performed. In order to verify the calculated spectra at room temperature, measurements of several flows of both species with no applied generator power were performed. The parameters of these measurements can be found in table 3.1. In order to validate the model at higher gas temperatures, additional measurements with an applied generator power of 50 W were performed. The parameters of these measurements can be found in table 3.2.

Table 3.1: Parameters of the measurements to verify the calculated spectra at room temperature.

Measurement	1	2	3	4	5	6	7	8	9	10
He/sccm	250	500	1400	250	500	1400	250	500	250	250
CH_4/sccm	0.3125	0.625	1.75	0.625	1.25	3.5	1.25	2.5	2.5	3.6
CH_4/He in %	0.125	0.125	0.125	0.25	0.25	0.25	0.5	0.5	1	1.44

Table 3.2: Parameters of the measurements with a generator power of $P = 50\,\mathrm{W}$.

Measurement	1	2	3	4	5	6
He/sccm	250	250	250	500	500	250
CH_4/sccm	0.3125	0.625	1.25	2.5	2.5	2.5
CH_4/He in %	0.125	0.25	0.5	0.5	0.5	1

Measurements with O_2 as an additional component of the gas are executed after assuring the validity of the calculated spectra. A constant helium flow of 250 sccm was chosen in order to provide the same residence time within all measurements. The CH_4 inflow was held constant at 0.625 sccm corresponding to 0.25% of the helium flow. In order to change the ratio of the admixted gases three different oxygen flows were chosen, namely 0.625 sccm, 1.25 sccm, and 2.5 sccm, corresponding to 0.25%, 0.5%, and 1% of the helium flow, respectively. To modify the plasma power of the discharge generator powers from 20 W to 70 W in steps of 10 W are applied.

3.5 Characteristics resulting from the utilized setup

Calibration approach

The density determined using the calculations is based on absorption calculations whereas the measurements using the FTIR are based on the absorbancy of the plasma. The absorbancy is defined as the decadic logarithm of the ratio of received and transmitted flux of a material while the absorption is described by the Lambert-Beer law given by equation 2.13. Dependent on the transmission, these two properties have certain ratios. Based on these ratios the density error caused by the use of the two properties can be corrected. At a transmission of 0.95, the magnitude observed in the experiments, the ratio of absorption to absorbance is 2.15. The determined densities are multiplied by this factor, yielding real measured densities.

Residence time

It is possible to determine the mean time of residence of a molecule inside the plasma volume from the geometry of the plasma chamber in combination with the amount of flowing gas. This time constant is independent on the density of the plasma, thus independent on a rise of the temperature of the system, and is evaluated to have a mean value of 81 ms. As the focus of the light coming from the FTIR is in the middle of the plasma chamber, the mean time a particle spends in the plasma before it is detected τ is only half of this value:

$$\tau = 40.5\,\mathrm{ms} \tag{3.1}$$

Calculating the plasma power

The energy deposited in a plasma is one of the most important parameters to characterize it. A VI probe was used to calculate the plasma power. The power is determined by the product of current and voltage with an additional factor determined by the shift between those two properties. The shift between the parameters results from the electrical components used and has a fixed value of Φ_0 in the case of no ignited plasma. The phase shift changes to a value of Φ in the case of an ignited plasma as the plasma can be interpreted as an additional electrical component. The change in the phase shift results from the impedance of the plasma and can therefore be directly connected to the plasma power P_{Pl}, following the expression:

$$P_{Pl} = U_{meas} I_{meas} \cos\left(\Phi - \Phi_0\right) \tag{3.2}$$

with the measured voltage U_{meas} and the measured current I_{meas}.
Due to the fact that the plasma is expected to be a static system the plasma power is assumed to vary around a constant value during the time of operation. Its value is estimated by the mean value of the calculated powers while its error is defined by the standard deviation of these values.

Determination of the model parameters

As mentioned in section 2.7.3 the free parameters of the modelled spectra are the density of a species as well as its rotational and vibrational temperatures. In order to determine the matching parameters in the calculation, a measured spectrum and a calculated one are plotted. They are complemented with the related residue as this property is useful for finding the best match of both spectra.

Each molecule has several, unique wave numbers in which its emission occurs, as absorption takes place around the normal vibrations of the molecules. The normal vibrations chosen for analysis in this study are displayed in table 3.3.

Table 3.3: Wave number ranges used to analyse the different species.

Species	CH_4	H_2O	CO_2	CO
ν/cm^{-1}	$2850 - 3200$	$1300 - 1900$	$2250 - 2450$	$2000 - 2300$
Normal vibration	ν_1	ν_2	ν_3	ν_1

The adjustments of the parameters were done starting with the density, proceeded by the rotational temperature with the vibrational temperatures being used to correct remaining perturbations.
A resulting spectrum with its residue is presented in figure 3.3.
It can be observed that the perturbations in the residue are orders of magnitude smaller than the measured peaks which indicates a good fit of the parameters. Global trends occurring in the residue are caused by other effects and have no relevance for the determined parameters.
For the rest of the study, this method is used to determine the densities and temperatures of the observed species in the performed measurements.

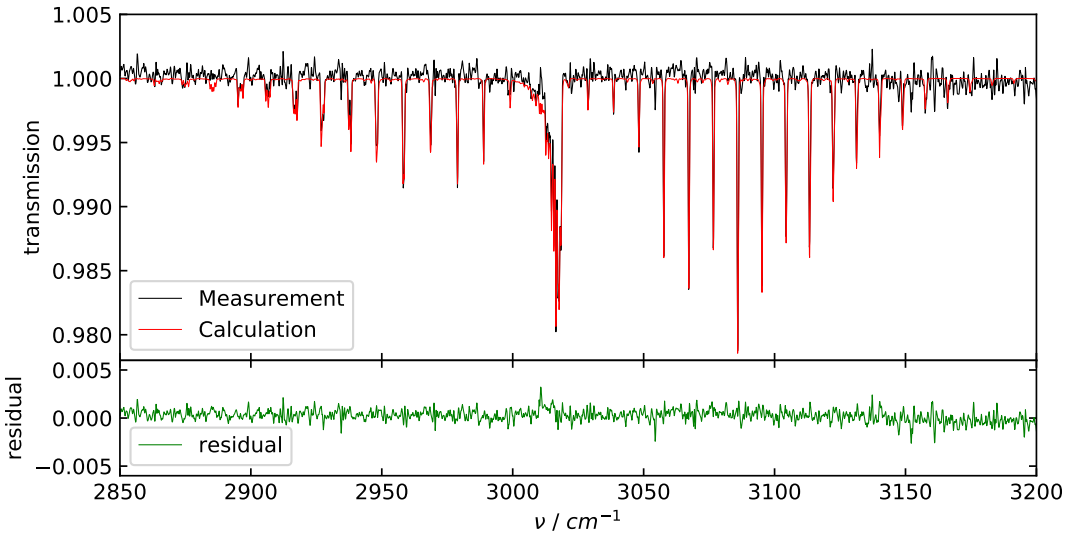

Figure 3.3: A measured and calculated CH_4 spectrum with the residue between the two spectra. The plasma parameters were inflows of 250 sccm He, 0.625 sccm CH_4, and 1.25 sccm O_2 with a generator power of 20 W.

4. Validation and analysis of pure CH_4 plasmas

In this chapter, the experiments performed with varying methane admixtures are analysed. At first, the signal is calibrated for a known CH_4 admixture. Ensuing that, densities and temperatures of plasmas ignited by a generator power of 50 W are examined. Eventually the yielded results are classified into the context of the study.

4.1 Analysis of methane densities without an ignited plasma

Figure 4.1 shows the CH_4 densities with no ignited plasma in dependence on the CH_4 admixture. Without ignition of the gas mixture all temperatures present are assumed to be at room temperature, thus 296 K. Hence the only free parameter within the modelled spectra was the methane density. As the influence of the density onto a spectrum is strong, rather large changes of the spectra are caused by a small change in density. Resulting from this the occurring density errors are small.

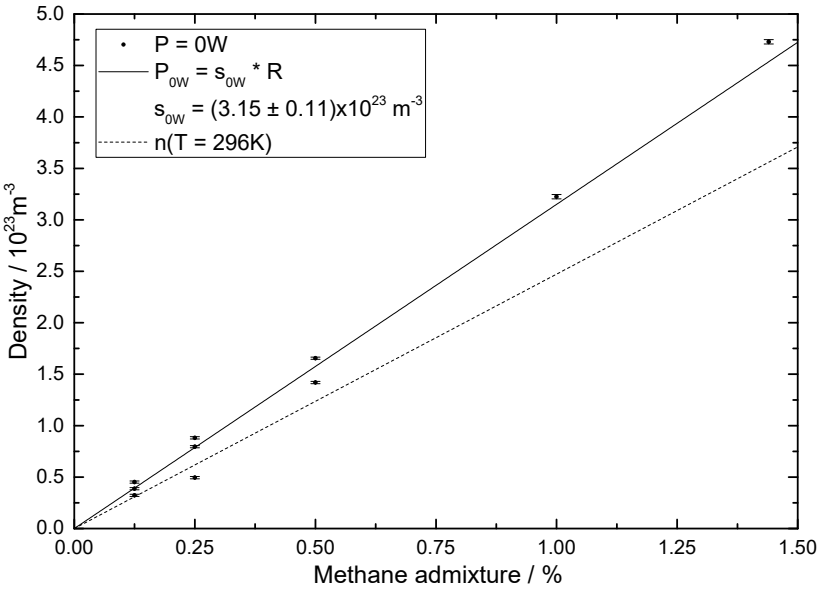

Figure 4.1: CH_4 densities in case of no applied power with a linear fit (solid line) and an expected slope for 296 K (dashed line).

If the total pressure within the plasma chamber is held constant, the methane density n is expected to obey the following trend:

$$n(x) = n_0 \left(\frac{x}{1+x} \right) \tag{4.1}$$

with the ratio of the methane to helium flow x and the density n_0 in case of $p_{CH_4} = 1$ bar. In case of a small methane admixture, thus $x \ll 1$, only the first non-vanishing term of the Taylor-expansion $n_0 x$ falls into account. Therefore, the densities in figure 4.1 were approached using a linear fit. The densities support this approach even though the chosen errors were underestimated. The underestimate of the density errors is amplified by the fact that error bars of different measurements do not overlap.

The densities plotted are those obtained from the comparison with calculated spectra. Those densities are corrected by effects caused by the used method of analysis but not physical effect present in the plasma chamber. In order to correct the densities by the latter mentioned effects, the methane density determined on base of the slope, is compared to a reference value. The reference value is calculated using the general gas equation at atmospheric pressure ($p = 1 \times 10^5\,\mathrm{Pa}$) and room temperature ($T = 296\,\mathrm{K}$). The reference density at 1% of CH_4 admixture is $2.47 \times 10^{23}\,\mathrm{m}^{-3}$. The correction factor is:

$$K = \frac{n_{ref}}{n_{meas}} = 0.78 \pm 0.03 \tag{4.2}$$

Due to the fact that the factor is below unity the density is overestimated. Within the plasma chamber several effects affect the density measurement. An effect leading to an underestimation of the density is the optical path of the infrared light. If the beam is focused to some extent, not the whole plasma volume is probed. As the total number of atoms is relevant for absorption but the volume assumed in the model is larger than the actual volume, the determined density is underestimated. An effect contributing to an overestimation of the density are total internal reflections. If a photon is reflected by the plasma chamber its total path length in the plasma volume extends. As more molecules for potential absorption are present in the longer beam path an absorption of the photon is more likely. The density has to be overestimated for the model in order to have the same amount of molecules in the path of one photon.
The correction factor results from an overlap of these effects. As the factor is below unity it can be deduced that total internal reflections are the dominant mechanisms leading to a distorted density. In the following, the displayed densities are calculated from the product of correction factor and determined density.

4.2 Analysis of methane densities with an ignited plasma

The CH_4 densities in case of an applied generator power of 50 W are plotted in figure 4.2. The red line refers to the best fit of the measured densities and the dashed black line corresponds to an expected density for a temperature of 370 K. This temperature was picked because it matches the observed rotational temperatures which are plotted in figure 4.3.

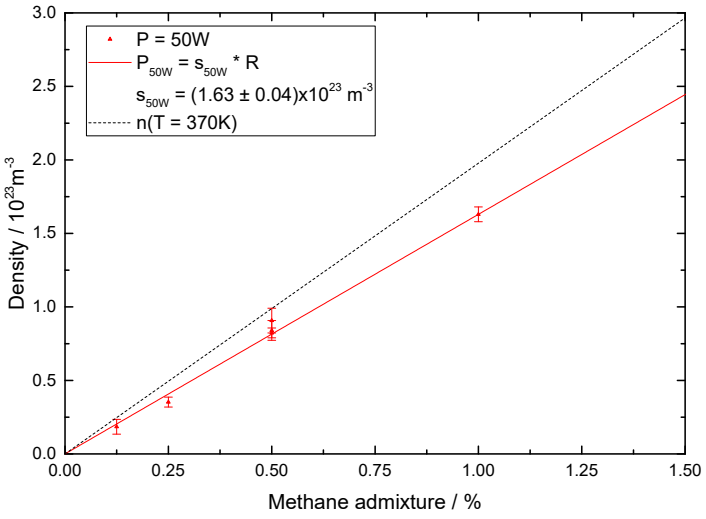

Figure 4.2: Measured densities with 50 W of applied power and a reference density at $T = 370\,\mathrm{K}$

The plotted data confirm the line of best fit and also the linear approximation of equation 4.1. The fact that the slope does not coincide with the one calculated based on the rotational temperatures, can be caused by two different mechanisms. The methane density can be either underestimated due to consumption of CH_4 by plasma chemistry or a false estimate of the gas temperature.
Taking a look at potential plasma chemistry happening the only potential reactant is methane, as helium is a noble gas which is expected to not react. From CH_4 the first molecule that is expected to be formed is CH_3 as it can be formed by detaching a hydrogen atom. From CH_3, either CH_2 or other hydrocarbons C_2H_X can be formed. These species can either be present in the plasma or lost by the plasma through surface interactions. The expected surface interaction of any hydrocarbon is coating of the plasma chamber. These interactions can be excluded as a cause of methane consumption as no significant coating was observed.
The absorption lines of other hydrocarbons than CH_4 lie in the same regions as those from CH_4 [20]. In the measured spectra no absorption that was higher than the background noise could be observed for other hydrocarbons. Therefore, it can be said that other hydrocarbons are formed with that low densities that the used method of analysis is impervious to them.
Thus, surface chemistry as a potential mechanism of methane consumption can be excluded whereas the formation of other hydrocarbons with low densities is expected.

The second mechanism being capable to cause an underestimation of the density is an underpredict of the gas temperature with a value of 370 K. This value was chosen based on the mean value of the rotational temperatures. The rotational temperatures are displayed in figure 4.3.

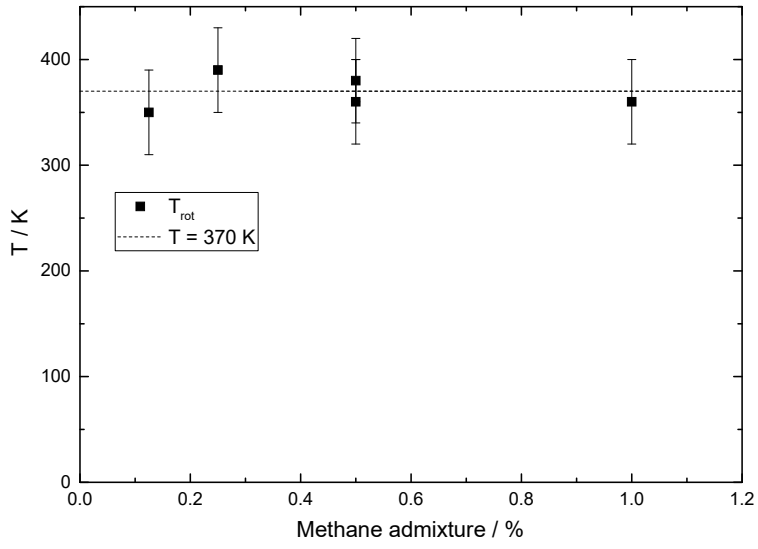

Figure 4.3: Determined rotational temperatures for the different admixtures with a mean value of 370 K (dashed line).

As no trend of the rotational temperatures with respect to CH_4 admixture can be observed it can be assumed that the rotational temperature is independent on the admixture. The mean value of the temperature of 370 K lies slightly above room temperature and in an area expected for the temperature of the plasma chamber. The low rotational temperature is caused by the fact that the momentum transfer between CH_4 and He atoms or electrons is inefficient due to the discrepancy between their masses. Therefore, the excitation of rotational degrees of freedom is inefficient, leading to rotational temperatures similar to the temperature of the plasma chamber.

The other temperatures present are the vibrational ones. These are plotted in the figures 4.4a and 4.4b. The error bars correspond to a temperature range in which the related spectrum shows small changes. The pairs of vibrational temperatures 1 and 3 as well as 2 and 4 show similar behaviours. The former two refer to stretching vibrations and have a mean temperature of 1000 K with no trend with respect to methane admixture. The latter two belong to bending vibrations with temperatures of around 370 K, thus in the region of the rotational temperature. They show no trend with respect to admixture either.

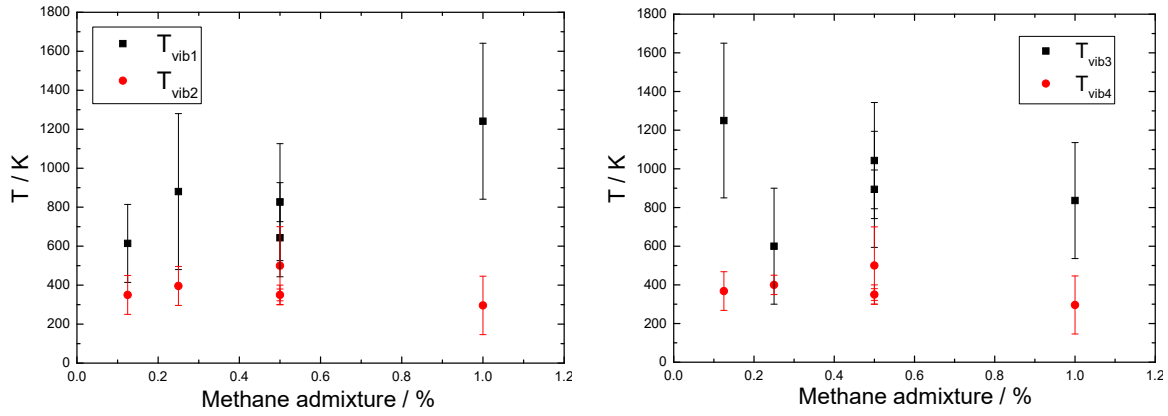

(a) T_{vib1} and T_{vib2} **(b)** T_{vib3} and T_{vib4}

Figure 4.4: Vibrational temperatures with 50 W of applied power.

The excitation of vibrational modes can either take place via Penning excitations by the collision with metastable helium atoms He^* or by vibrational pumping. As the density of helium metastables is independent on the methane admixture, no trend of Penning excitations with respect to methane admixture is expected. Due to vibrational pumping only taking place through collisions with other methane molecules it is expected to be more effective in cases of higher methane admixtures. The quenching of methane is expected to be more present for higher methane admixtures as it scales with the methane admixture as well. With more methane molecules being present the number of potential quenching partners increases which leads to a more effective cooling of the excitation modes. Therefore, any temperature trend with respect to admixture is caused by the total of vibrational pumping and quenching. As in none of the temperatures a trend is present Penning excitations can be identified as the main mechanism of excitation. No other propositions about quenching and vibrational pumping other that their sum being close to zero can be made, as both mechanism scale with admixture.

Electron impact excitations of stretching vibrations are effective as the electronic excitation causes a change in the wave function of the molecule. This leads to the excitation of a stretching vibration. Therefore, the temperatures of the two vibrational stretching modes ν_1 and ν_3 are high due to the high electron temperature. Due to the fact that the influence of the stretching vibrations onto the methane spectrum is weak the errors of those are rather large. Hence, it can be said that stretching vibrations are almost entirely excited by electron impact excitations with temperatures in the order of 1000 K.
Excitations of bending vibrations are done via momentum transfer in the collision with other particles. Due to the high ratio of molecular mass to electron mass a momentum transfer between those two species is inefficient. Therefore, no internal excitations of the bending excitations ν_2 and ν_4 take place. From that and the high inflow of cold CH_4 molecules it can be expected that the temperatures of the bending vibrations are similar to the temperature of the plasma chamber. Thus, it can be expected that the temperature of the bending vibrations coincide with the rotational temperature: $T_{vib1} = T_{vib2} = T_{rot}$.

With the explanation of the excitation mechanisms of the different vibrational modes being presented and two vibrational temperatures coinciding with the rotational temperature it can be justified that the plasma temperature coincides with the rotational one. As the reference density was calculated using the mean value of the rotational temperature without its error being taken into account, a small underestimate of the density can be caused by an underestimate of the rotational temperature.

Based on the provided explanations the underestimate of the density is caused by the sum of two effects. The first one is the formation of other hydrocarbons than CH_4 which consumes CH_4 leading to a smaller density of it. The other one is an underestimate of the rotational temperature caused by its large error margin.

4.3 Conclusion and context for the further study

Measurements using helium as a buffer gas with methane admixtures ranging from 0.125% to 1.5% with and without an applied generator power were performed.
Densities determined with no applied power confirmed the approach of a linear fit to densities in case of low admixtures. As the error ranges of measurements with the same parameters did not overlap, an underestiamte of the density errors was deduced.
Based on a reference density a correction factor of 0.78 ± 0.03 was determined. This factor corrects physical effects occuring in the plasma chamber and is specific for the used setup. The determined value is used in the further study to correct determined densities.

In case of plasmas ignited by a generator power of 50 W the trend of densities with respect to methane admixture is linear as well. A methane density of $(1.63 \pm 0.04) \times 10^{23}\,\mathrm{m}^{-3}$ for 1% methane admixture was determined. This density is lower than the earlier used reference density due to the higher temperature of the system. An approach to this density using the mean value of the rotational temperature (370 K) yielded an overestimate of the density. Surface chemistry is neglected as a cause due to no coating of the plasma chamber being observed. The difference in density is ascribed to the formation of hydrocarbons in the plasma as well as an underestimate of the rotational temperature.

The temperatures of the two stretching vibrational modes ν_1 and ν_3 are determined to be in the region of 1000 K. As the main excitation mechanism Penning excitations are determined. The bending vibrations ν_2 and ν_4 show temperatures in the region of the rotational temperature which is caused by the temperature of the plasma chamber due to the inefficient momentum transfer between electrons and molecules.
From these results the identification of the plasma temperature with the chamber temperature can be confirmed. The combination of an underestimate of the rotational temperature and the formation of other hydrocarbons as an explanation for the discrepancies in the densities is proposed.

In the further context of the study no issues due to an underestimate of the rotational temperature occur as the densities are the main parameter used for analysis. Any error present in the rotational temperature has only small influences onto the densities and causes perturbation smaller than the errors of the densities themselves.
For further studies focussing on the temperatures in the observed kind of plasmas, it is recommended to implement an additional measurement of the temperature of the system to compare it to the rotational one.

5. Analysis of CH_4/O_2 Plasmas

The following chapter contains an analysis of plasmas with CH_4 and O_2 admixtures. Plasma powers with respect to generator powers are examined. Following that, the trends of different species with respect to plasma powers are analysed. Based on the obtained densities as well as balances of individual atoms, a chemical reaction is proposed and verified using a global chemistry model. From comparison of a global model with the measurements a correlation between electron density and plasma power is derived.

5.1 Plasma power characteristic

In order to characterize the observed plasmas the dissipated power with respect to generator power is analysed. The determined plasma powers for the different admixtures are presented in figure 5.1. The values themselves are time averaged values calculated using equation 3.2 with their error being determined by their standard deviation.

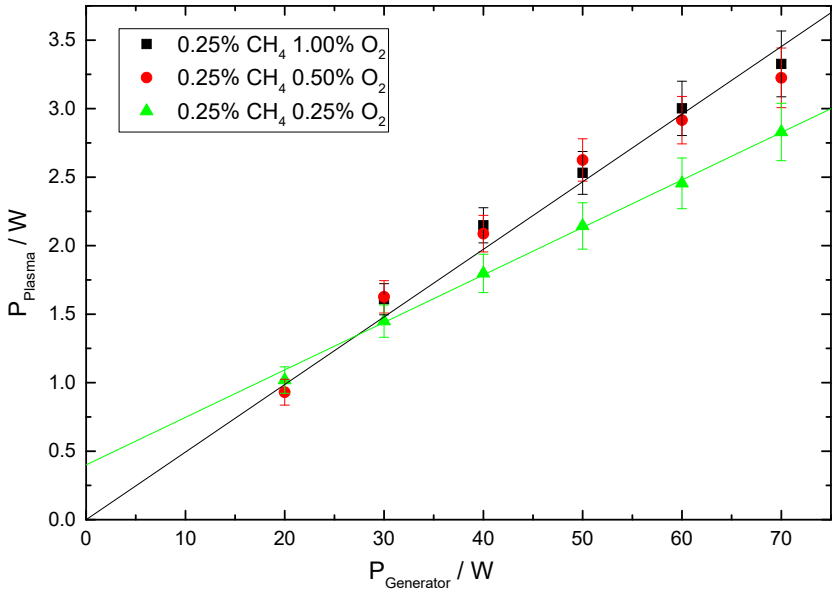

Figure 5.1: Measured power characteristics of the plasmas for different O_2 admixtures with a combined estimation line for the cases of 0.5% and 1% oxygen admixture (black) and one for 0.25% oxygen admixture (green).

The data are expected to follow a linear behaviour as the plasma acts like an electrical component within the electric circuit. With more generator power being applied the power loss by each of the electrical components increases. In case of an constant resistance of the plasma the plasma power is linear dependent on the generator power. Following that, it can be deduced that the data are expected to cross the origin of coordinates.
In order to check this behaviour for oxygen admixtures of 0.5% and 1%, a black line as guide to the eye was plotted in figure 5.1. This line obeys the predicted behaviour. It can be assumed that the resistances in the two cases are constant and approximately equal. As the only difference between the two plasmas is the oxygen admixture, it can be said that an oxygen admixture in the range from 0.5% and 1% does not change the resistance of the plasma, regardless of plasma powers within the examined region.
By taking a look at the line in case of 0.25% of oxygen admixture it can be seen that the linear behaviour is described well whereas the y-intersection is contrary to the expectations. Furthermore, the slope is less steep. Hence, the resistance of these plasmas

was constant but lower than in the other cases. As the transit through the origin of the coordinates is a fixed boundary condition it is expected that the linear behaviour does not hold true for generator powers below 20 W. As the plasma can not be ignited for too low plasma powers, a rapid drop in plasma power is expected in this region. Due to the fact that the slope is less steep, it can be deduced that plasmas with oxygen admixtures of 0.25% have a different resistance than those with higher admixtures. Therefore, a shortage of oxygen evokes a different resistance of the plasma.

5.2 Analysis of the densities

In this section the densities of the observable species, depending on different oxygen admixtures, are analysed. The trends as well as absolute densities are compared and explained based on the parameter oxygen admixture. Based on the observed trends predictions about the plasma chemistry are deduced.

5.2.1 Plasmas with an admixture of 1% and 0.5% of oxygen

The density trends in case of an oxygen admixture of 1% are plotted in figure 5.2 with the plasma power forming the x-axis. A trend of the different species with respect to plasma power can be observed. While the CH_4 density drops with an increase in the plasma power, the total density of the other measured species increase. The H_2O and CO_2 densities show an increase with plasma power but with different slopes, the CO densities are constant in terms of plasma power.

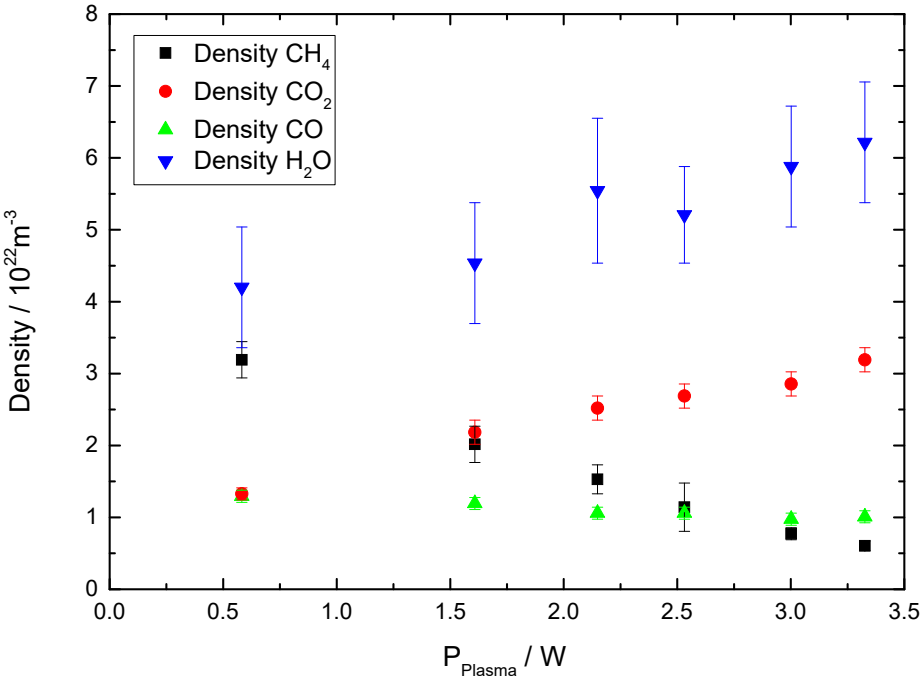

Figure 5.2: Determined densities for the different species in case of an oxygen admixture of 1%.

The decrease of the density of CH_4 is explained by the energy deposited in the plasma. With higher plasma powers more energy is available for different processes in the plasma to happen. One of these processes are chemical reactions which require activation energy. With more energy being deposited the number of molecules that are provided the necessary activation energy increases, which leads to higher reaction rates. With more chemical

reactions taking place, more of the reagents are consumed leading to lower densities. With higher plasma powers, thus more energy deposited in the plasma, the measured methane density decreases, indicating that it is a reagent. For higher plasma powers more methane is consumed, which leads to a lower density. As the reaction rate is dependent on the methane density it decreases. Due to this effect the consumption of methane does not scale linear with plasma power but is determined by a balance of the two effects that have an influence on the reaction rate.
The density trends of CO_2 and H_2O are reversed to the one of CH_4. With higher plasma powers their densities increase with the slope describing H_2O being more steep. An increase of the density with plasma power is typical for a product of a chemical reaction. Due to the additional energy supplied by a higher plasma power the reaction rates increase, hence leading to more of the products being formed. Due to the products being stable in the context of the plasma no reactions consuming them are present. As the steepness of a density trend is directly related to the absolute densities it can be used to estimate the formation of the related species. With the trend of H_2O being more steep than the one of CO_2 it can be concluded that H_2O is more efficiently formed than CO_2.
As the density of CO shows no dependency on plasma power, it does neither match the behaviour of a reagent nor a product. In order to show a constant density it needs to be produced with the same rate as it is consumed. Thus it takes the role of an intermediate product. From some of the products being known, it can be assumed that CO is a precursor in the formation of CO_2.

The density trends in case of an oxygen admixture of 0.5% are presented in figure A1.1 in appendix A1. The different species show similar behaviours as in figure 5.2. The CH_4 density decreases with an increase of plasma power while those of H_2O and CO_2 increase. Again this is caused by the additional energy being provided by higher plasma powers. The constant behaviour of CO in figure A1.1 in appendix A1 emphasizes its role as an intermediate product in the formation of CO_2. The fact that the absolute densities of the different species in figure A1.1 are similar to those displayed in figure 5.2, implicates that enough reactant in the form of O_2 is provided.

5.2.2 Plasma with an admixture of 0.25% of oxygen

The species' densities in case of an oxygen admixture of 0.25% are plotted in figure 5.3. In general, the figure supports the observations of CH_4 being a reagent, CO_2 being a product, and CO being an intermediate product in the formation of CO_2. Due to the fact that the errors in the H_2O density are large no statement about its trend can be deduced.

For plasma powers larger than 2 W no dependency of the density on the plasma power can be observed. If one compares the densities for plasma powers below 2 W with those in figure 5.2, the values are the same. Therefore, the energy provided by a plasma power of 2 W is sufficient to consume an oxygen admixture of 0.25% via the oxidation of methane admixed with 0.25% as well. Taking a look at higher plasma powers than 2 W the densities in case of the lowest oxygen admixture start to vary from those observed in cases of higher admixtures. As the plasma power correlates with the energy deposited in the system, the plasmas with an oxygen admixtures of 0.25% can not convert more than a power of 2 W through reactions including methane. This limiting value is caused by a lack of the other reagent O_2 which is almost entirely consumed. The power excess is deposited in other mechanisms than plasma chemistry which reduces the energy efficiency of the process.

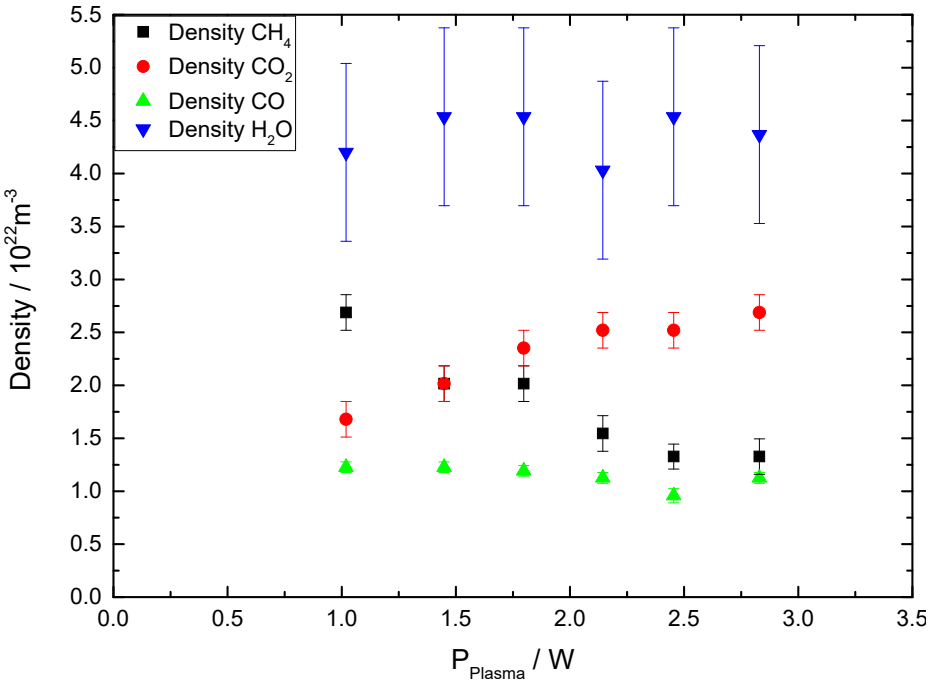

Figure 5.3: Determined densities for the different species in case of an oxygen admixture of 0.25%.

5.3 Carbon balance

The measured species containing carbon are CH_4, CO_2, and CO. As no direct reaction from the first one into the latter two exists intermediate products have to be formed. In order to estimate the amount of carbon present in intermediate products the sum of the densities of the measured carbon containing species is displayed in figure 5.4. The solid line represents a linear fit to all measured densities. Additionally, a reference value at $P = 0\,\mathrm{W}$ obtained from figure 4.1 and densities based on the rotational temperatures of CH_4 in case of an oxygen admixture of 1% are plotted. Using the reference point a trend line (dashed) is plotted which is used to indicate the amount of carbon present in intermediate products.

The total densities for the three different admixtures are located in the same region with lower densities being present at higher plasma powers. Due to the fact that no differences are observed it can be deduced that the formation of intermediate products is independent on the oxygen admixture. In the region up to 2 W this was expected as no difference in the densities between the figures 5.2, A1.1, and 5.3 were observed.

In cases of plasma powers above 2 W a change in the amount of intermediate products between the different admixtures is expected. This change is caused by the fact that the amount of consumed methane is different for the different oxygen admixtures above 2 W of plasma power. In figure 5.4 this can not be observed as the difference in methane consumption is smaller than the error bars of the densities.

The densities calculated on base of the rotational temperatures lie in the same region as the measured ones. Therefore, a decrease of the total density with increasing plasma power is caused by a heating of the plasma chamber. On the one hand this confirms the consistency of the rotational temperatures with the determined densities, on the other hand this enables an estimate of the amount of intermediate products. The rotational temperature correlates with the total density, whereas the plotted densities only represent the sum of the densities of CH_4, CO_2, and CO. Therefore, the difference between them corresponds to the total density of intermediate products. The density itself can not be described due to the large errors, but it can be estimated that less than 10% of the carbon

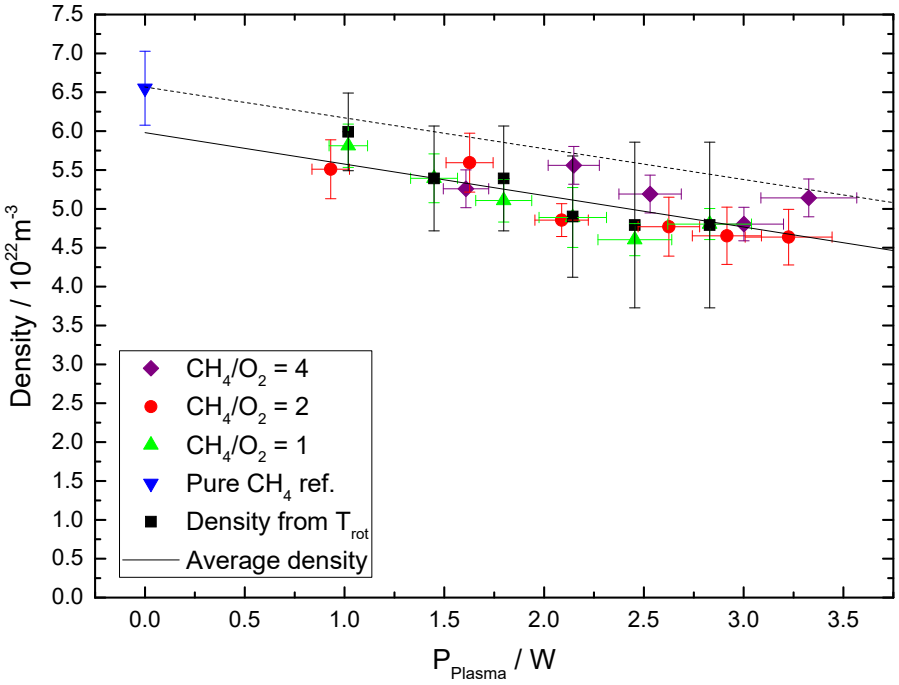

Figure 5.4: Carbon balance of the combined measurements with densities calculated from the rotational temperatures in case of an oxygen admixture of 1% (black), a reference value from the measurements without applied power (blue), a density fit to the measurements (solid line), and an estimation line for the deficit (dashed line).

is bound within intermediate products.
In order to confirm this estimate a comparison with a reference value at $P = 0\,\mathrm{W}$ is done. This reference value is plotted in figure 5.4 as well. In order to be able to compare density values at 0 W an extrapolation of the measured densities down to this value had to be done. Because these values showed a linear behaviour within the region of the measurements, the extrapolation was done using a linear fit. In order to estimate the amount of intermediate products a dashed line crossing the reference point is plotted parallel to the extrapolation line. The difference between the two lines arises from the deficit of carbon contained in intermediate products. This deficit confirms the estimate of less than 10% of the carbon being bond in intermediate products.

Based on these observations it can be deduced that CH_4 and CO_2 are the only non-intermediate, carbon containing species. The intermediate product with by far the highest density is CO. Following these observations, it can be said that CH_4 O_2 plasmas are capable of forming CO_2 with no other carbon based final products being formed. The amount of carbon contained in intermediate products is small and independent on the oxygen admixture within the analysed parameters.

5.4 Determination of the total reaction

The other species present in both, educts and products, is hydrogen. In order to check its balance the sum of the methane density and the half water density is plotted in figure 5.5. The water density was bisected as the hydrogen provided by one methane molecule is sufficient to form two water molecules. The densities obtained from the rotational temperatures as well as the reference value used in figure 5.4 are plotted in figure 5.5 as well.
Again, the densities referring to the different oxygen admixtures match, indicating that intermediate products are independent on an oxygen admixture within the chosen range

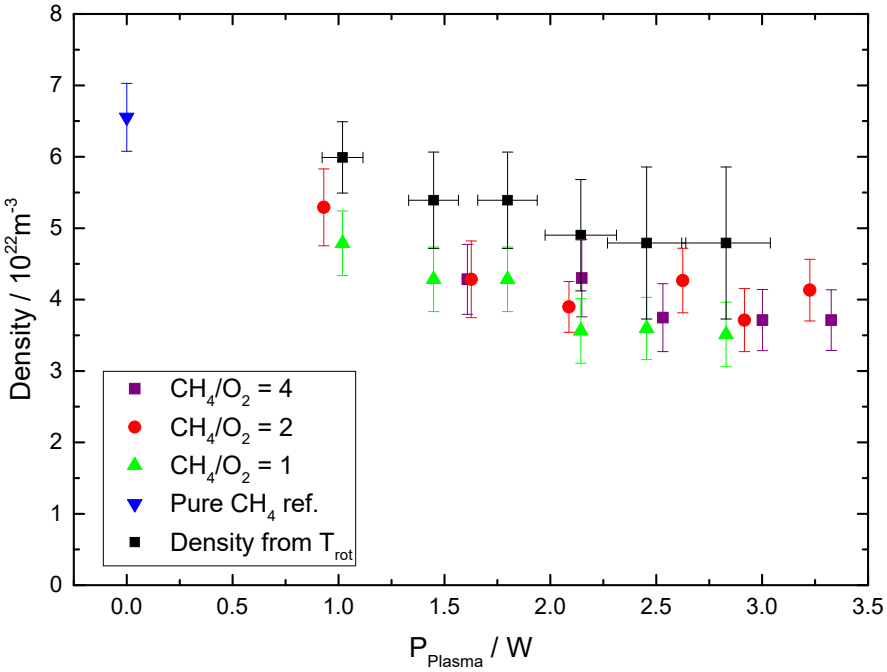

Figure 5.5: Hydrogen balance based on the sum of the methane density and the half water density together with a reference value at 0 W (blue), and densities based on the rotational temperatures in case of 1% of oxygen admixture (black).

of admixtures. The densities based on the rotational temperatures refer to a density decrease as it is expected due to heating of the plasma. The measured data points proceed below these which indicates that significant amounts of hydrogen are not detected. This hydrogen can be either contained in intermediate products or molecular hydrogen is formed. As the measured densities proceed parallel to the calculated densities it can be deduced that the amount of undetected hydrogen is independent on the plasma power. In the domain below 2 W this was expected as the same amount of methane is consumed for the different oxygen admixtures. As in the carbon balance the expected differences in densities of the intermediate products in the region above 2 W due to the different amount of methane being consumed can not be observed. Equivalent to the case of the carbon balance this is caused by the large error bars in comparison to the small differences in densities.
From the comparison of the absolute densities in case of the calculated sum and the estimate based on the rotational temperature, it can be deduced that around 25% of the hydrogen is not detected. This value is high in comparison to the one determined in the carbon balance. This difference may be explained by the formation of molecular hydrogen which can not be observed as it is infrared inactive.

Based on the carbon and hydrogen balances the following reaction can be identified as the overall reaction in the plasma:

$$CH_4 + 2\,O_2 \rightarrow CO + X \rightarrow CO_2 + 2\,H_2O \tag{5.1}$$

with X *denoting any kind of intermediate product.* A factor of 2 in front of O_2 and H_2O was chosen as it refers to the case of methane being consumed entirely, i.e. a maximal necessary amount of oxygen admixture. In the experiment this value corresponds to an oxygen admixture of 0.5%. In the related densities in figure A1.1 in appendix A1 no full conversion could be observed due to the statistical character of the reaction and the finite residence time. As the residence time of the molecules within the plasma is finite some of the initial as well as intermediate products will leave the chamber before forming the final products. Therefore, some of these species such as CO can be observed in the measured

spectra. Other intermediate products can not be observed as they are either not infrared active or formed in a density below the sensitivity of the used method.

5.5 Comparison with a global chemistry model

In order to understand the observed behaviour of the plasma better and to deduce further results from the measurements, a global model describing the plasma chemistry is used. Its principle is briefly described in appendix A2. The aim of the model is to recreate the single steps of the reaction described by equation 5.1. The reactions used in the model are displayed in table 5.1.

Table 5.1: Reactions used in the global model with their rate coefficients and temperature intervals of validity.

Reaction			Rate coefficient $m^3 molecule^{-1} s^{-1}$	Temperature K	Reference
$O_2 + e^-$	$\rightarrow$	$O + O$	1.95×10^{-15}	$300 - 2500$	[21]
$O + e^-$	$\rightarrow$	$O(^1D)$	2.02×10^{-15}	$300 - 2500$	[22]
$CH_4 + O(^1D)$	$\rightarrow$	$CH_3 + OH$	1.40×10^{-16}	-	[4]
$CH_3 + O$	$\rightarrow$	$CH_2O + H$	1.30×10^{-16}	$300 - 2500$	[21]
$CH_3O + OH$	$\rightarrow$	$CH_2O + H_2O$	3.00×10^{-17}	$300 - 2500$	[21]
$CH_3O + CH_3O$	$\rightarrow$	$CH_3OH + CH_2O$	1.00×10^{-16}	$300 - 2500$	[21]
$CH_3OH + O$	$\rightarrow$	$CH_2OH + OH$	5.56×10^{-21}	$298 - 998$	[23]
$CH_3OH + OH$	$\rightarrow$	$CH_2OH + H_2O$	2.17×10^{-18}	$300 - 2500$	[24]
$CH_2O + H$	$\rightarrow$	CH_3O	1.00×10^{-16}	-	[25]
$CH_2O + OH$	$\rightarrow$	$HCO + H_2O$	3.02×10^{-18}	$200 - 2500$	[21]
$CH_2OH + O_2$	$\rightarrow$	$CH_2O + HO_2$	4.02×10^{-21}	$300 - 700$	[26]
$CH_2OH + HCO$	$\rightarrow$	$CH_3OH + CO$	2.00×10^{-16}	$300 - 2500$	[24]
$HCO + O$	$\rightarrow$	$CO + OH$	5.00×10^{-17}	$300 - 2500$	[21]
$HCO + O$	$\rightarrow$	$CO_2 + H$	5.00×10^{-17}	$300 - 2500$	[21]
$CO + O(^1D)$	$\rightarrow$	CO_2	8.00×10^{-17}	$100 - 2100$	[27]
$CO + OH$	$\rightarrow$	$CO_2 + H$	3.79×10^{-20}	$300 - 3150$	[28]
$CO + HO_2$	$\rightarrow$	$CO_2 + OH$	6.46×10^{-20}	$300 - 2500$	[29]

The electron impact reaction rates were exclusively obtained from the lxcat-database [30], the reaction rates of neutrals and radicals were based on rates used by Zhou et. al [4] and complemented by data from the NIST chemical kinetics database [25]. The electron impact dissociation of CH_4 was not taken into account as only data for combustion are provided. Due to the temperature of combustion processes being above 1000 K and the temperature of the observed plasma being significantly lower, it is expected that no electron impact dissociation of CH_4 takes place. Reactions in table 5.1 with no given temperature were derived experimentally for the oxidation of methane in setups with similar electron temperatures. Therefore, the rate of these can be used in this study.
The initial parameters of the calculations are a filled chamber with a helium density of $2.4 \times 10^{25}\,m^{-3}$, a methane density of $6 \times 10^{22}\,m^{-3}$, and oxygen densities of 0.6×10^{23} sccm, 1.2×10^{23} sccm, or 2.4×10^{23} sccm dependent on the chosen admixture in the reference experiment. The inflow of the species is chosen based on the experiment which is be modelled. Volume and surface were respectively chosen to $3.74 \times 10^{-7}\,m^3$ and $1.4 \times 10^{-3}\,m^2$ due to the geometry of the used plasma chamber.
In the global model, the trend of partial pressures of the different species with respect to time is calculated. Based on the partial pressures it is possible to calculate densities using

the general gas equation assuming a certain temperature. As the temperature is a global parameter which can be approximated using rotational temperatures, the temperature is chosen to be the mean value of the rotational temperatures of all species, excluding H_2O. H_2O is excluded as its temperatures could not be determined. A temperature value of 400 K was obtained using this method which allows the calculation of the densities of the different species.
The free parameter within the global model is the electron density. Due to the high pressure of the plasma, the electron density is expected to be in the order of $2 \times 10^{16}\,\mathrm{m}^{-3}$. Therefore, the global model was run at various electron densities ranging from $1 \times 10^{16}\,\mathrm{m}^{-3}$ to $3 \times 10^{16}\,\mathrm{m}^{-3}$ with intervals of $0.5 \times 10^{16}\,\mathrm{m}^{-3}$ with parameters matching the modelled experiments.

An example of the time trend of partial pressures is plotted in figure 5.6. The vertical line is plotted at $t = 40.5$ ms, the mean residence time of a molecule before detection. The unit of the y-axis is in bar, thus an admixture of 1% refers to a partial pressure of 1×10^{-2} bar. Relating to the plot it can be observed that the underlying reactions correspond to the reaction proposed based on the measurements. CH_4 and O_2 are consumed while CO_2 and H_2O are produced. The plot also shows that for all species a saturation is formed after long times. After 20 ms a peak in the CO density is present.

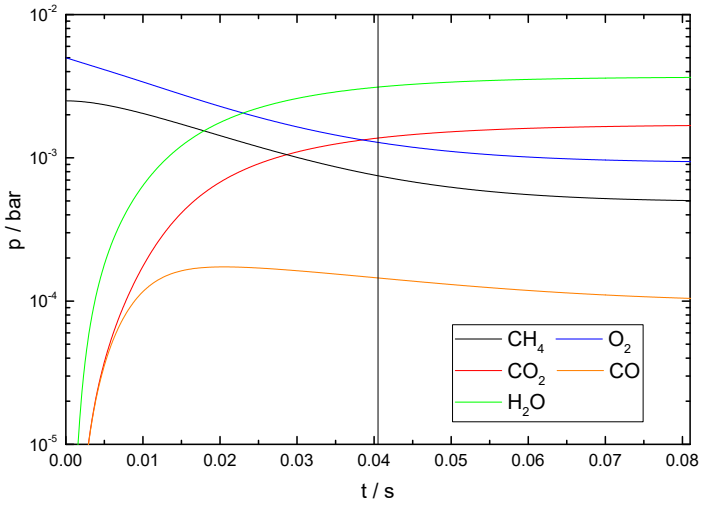

Figure 5.6: Density trends of different species in case of $n_e = 2 \times 10^{16}\,\mathrm{m}^{-3}$ and an oxygen admixture of 0.5%.

These observations can be described by the way the global model works. In the beginning only reagents are present. O_2 starts to get dissociated and $O(^1D)$ radicals are formed. As these are necessary for reactions of CH_4, the partial pressure of it starts to decrease with a delay. After 20 ms the reaction rate of CH_4 molecules is at its maximum. From the resulting products, CO is formed resulting in a peak at the same point in time. As less CH_4 is present after this peak the density of CO decreases due to its consumption in the formation of CO_2. During the whole progress H_2O is formed from OH radicals which detach a hydrogen atom from one of the CH_4 based products. Due to the fact that CO_2 and H_2O are final products their partial pressure rises constantly.
The equilibrium after around 70 ms results from the convection implemented in the model. In the equilibrium, the production of a species by reactions and the loss of it by convection are equal. As convection is small the reaction rates have to drop by several orders of magnitude. This decrease in reaction rate is caused by the remaining densities of the initial particles being low. Relating to the experiment this equilibrium can be expected near the exhaust of the plasma chamber as the total residence time was determined to 81 ms. The parameter electron density mainly influences the time scale of the reactions

as the reaction rates of electron driven reactions directly scale with it.

In the measurements the main influence parameter onto the densities was the plasma power, whereas the results obtained from the global model are dependent on the electron densities. Therefore, a correlation between these two parameters has to exist. The measurements constitute real values, while the densities resulting from the global model are arbitrary. So one has to match electron density to measured plasma power.
The comparison of the densities obtained by measurements with those received from the global model was done by analysing the ratio of them. Densities for four different species were measured, which means that four related ratios could be analysed at a time. As the aim was to match an electron density used in the model to a measured plasma power, matching pairs of these two parameters had to be found. A matching pair was defined as the pair of electron density and plasma power which yields the same densities for all species. In order to find this pair of values the electron density was held constant while the plasma power is varied.
For each electron density, densities for the different species were calculated. These were then divided by the densities measured in the experiment with matching parameters. One set of calculated densities was divided by the densities measured for the different plasma powers separately. Based on these calculations ratios of the different species at the different plasma powers were obtained. The ratios were then plotted in single figures. In case of an oxygen admixture of 0.5% and electron densities in the range from $1.0 \times 10^{-16}\,\mathrm{m}^{-3}$ to $3.0 \times 10^{-16}\,\mathrm{m}^{-3}$, the resulting plots are displayed in figure 5.7.
The ratios describing the methane densities are small for low plasma powers and high for large plasma powers. This trend is based on the fixed electron density used in the global model. If the plasma power is too low for a chosen electron density, the methane density in the model is underestimated, yielding a too low ratio. If the plasma power is too high, the density calculated in the model is overestimated, leading to a too high ratio. The products CO_2 and H_2O show a reversed trend. If the plasma power is too low for the chosen electron density, the density of the products in the global model are overestimated, yielding a too high ratio. If the plasma power is too high, too few products are formed in the global model, leading to a low ratio.
Based on these considerations it is obvious that a matching pair is present if the ratios of all species coincide. In this case the electron density in the global model matches the plasma power in the experiment. As both methods produce densities matching real values, the ratios of all species are expected to coincide at a ratio of unity.
Taking a look at the plots in figure 5.7, it can be noticed that CO does not match the described trend but has a ratio below unity. Therefore, CO has to be excluded from the definition of a matching pair and only the remaining three species are taken into account. The underestimate of the CO density in the global model is caused by the missing implementation of CO_2 conversion. CO_2 conversion is mainly driven by He^* which are excited by free electrons. Due to the fact that the density of these metastables was not known this mechanism of CO production could not be implemented.
Taking a look at the ratios of the other species in figure 5.7, the expected behaviour of a jointly intersection at a ratio of unity is fulfilled in cases of lower electron densities. In case of the highest electron density no intersection takes place in the observed range from 0.75 W to 3.5 W. As the ratios do not follow a linear trend, an extrapolation into regions of higher plasma powers is not possible. Therefore, only four matching pairs of electron density and plasma powers could be deduced from figure 5.7.
Plots that are suited to obtain matching pairs in cases of other oxygen admixtures are displayed in figure A1.2 in appendix A1. In case of an admixture of 0.25% and electron densities below $2 \times 10^{-16}\,\mathrm{m}^{-3}$ the ratios describing the products were lower than unity. This behaviour is observed as the plasma powers matching those energy densities lie in

the range from 0 W to 0.75 W which is not covered by the measured data. In case of the highest oxygen admixture of 1% and electron densities above $1 \times 10^{16}\,\mathrm{m}^{-3}$ the ratios describing CH_4 were zero as the methane was fully consumed in the global model. Therefore, no matching pairs could be deduced for these cases.

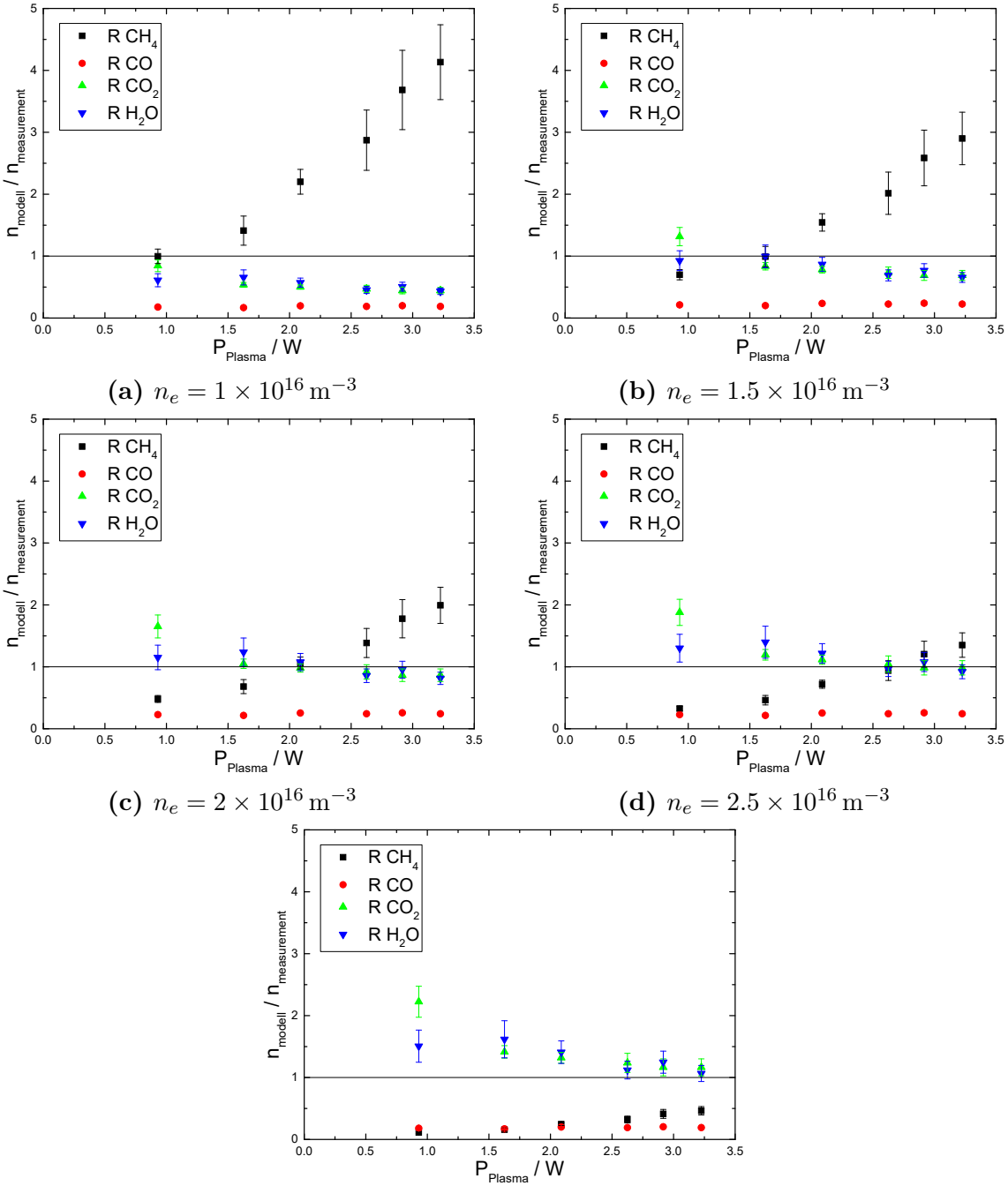

(a) $n_e = 1 \times 10^{16}\,\mathrm{m}^{-3}$ **(b)** $n_e = 1.5 \times 10^{16}\,\mathrm{m}^{-3}$

(c) $n_e = 2 \times 10^{16}\,\mathrm{m}^{-3}$ **(d)** $n_e = 2.5 \times 10^{16}\,\mathrm{m}^{-3}$

(e) $n_e = 3 \times 10^{16}\,\mathrm{m}^{-3}$

Figure 5.7: Ratios of modelled to measured densities in case of an oxygen admixture of 0.5%. The horizontal lines indicate the expected value of intersection.

The matching pairs of electron density and plasma power that could be derived from the figures 5.7 and A1.2 are plotted in figure 5.8. For the oxygen admixtures with more than one data point, a linear fit of the data is applied. These linear fits have a fixed y-intersection at 0 W as no free electrons are expected with no plasma power being applied. In case of the highest oxygen admixture only one value could be derived. As no linear fit could be applied, a line connecting the data point with the origin is drawn. This line gives a rough estimate of electron densities in case of oxygen admixtures of 1%.
In general, the electron density is expected to have a linear correlation with respect to

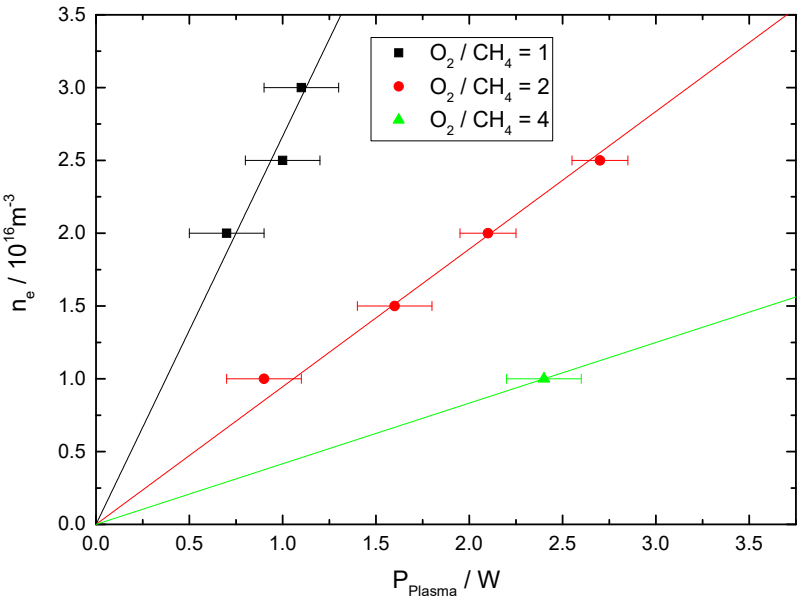

Figure 5.8: Electron density dependency on the plasma power for the plasmas of different oxygen admixtures. The black and red lines refer to linear fits forced through the origin, the green one was implemented to obtain an estimate of steepness.

plasma power. With an increase in plasma power, more energy is provided. An approximately constant percentage of the energy is expended in ionisation of atoms or molecules which leads to a linear rise in electron density. Adapted from this, it results that no free electrons are present without an applied plasma power.
The data, the two fitted lines are based on approve the linear behaviour as well as the y-intersection at 0 W. At the same plasma power, both of these plasmas obtain the same amount of energy per second, leading to the same number of free electrons being formed. In order to explain the discrepancy between the two slopes, an additional oxygen dependent mechanism which reduces the electron density has to be present. This mechanism may be the formation of O^--ions. These ions are formed from free electrons and oxygen radicals. The electron density decreases due to the fact that the consumed electrons are lost for plasma chemistry. As oxygen radicals are necessary for the formation of O^--ions, their formation is more likely in cases of higher oxygen admixtures, leading to lower electron densities in these cases.
Based on the slope in case of the highest oxygen admixture no isolated results can be deduced as it is not obtained by a fit, but as the value matches the expectations well, it can be assumed that it is valid in the context of the study.
The slopes of the different fits have the following values:

$$s = \begin{cases} O_2/CH_4 = 1 & (2.67 \pm 0.10) \times 10^{16}\,\mathrm{m^{-3}W^{-1}} \\ O_2/CH_4 = 2 & (9.5 \pm 0.3) \times 10^{15}\,\mathrm{m^{-3}W^{-1}} \\ O_2/CH_4 = 4 & 4.16 \times 10^{15}\,\mathrm{m^{-3}W^{-1}} \end{cases}$$

As mentioned, the different slopes are caused by the different amounts of oxygen radicals. By taking a look at the product of the O_2/CH_4 ratio and the referring slope, it can be seen that the values for the various cases are different. This is caused by the non-linear correlation between oxygen admixture and oxygen radicals. In case of the lowest oxygen admixture most of it is consumed by reactions with methane based products. This leads to a low density of oxygen radicals and the formation of only few O^--ions. In cases of higher oxygen admixtures roughly the same amount of oxygen is consumed. Due to the fact that the total amount of oxygen is larger, the density of oxygen radicals is significantly higher which leads to higher formation rates of O^--ions. The more excess of oxygen

is provided within the plasma, the more O^--ions are formed, resulting in lower electron densities.

5.6 Perspective for further studies of CH_4 O_2 plasmas

Measurements using helium as a buffer gas with a methane admixture of 0.25% and an oxygen admixture ranging from 0.25% to 1% and plasma powers ranging from 0.75 W to 3.5 W were performed.

The plasma power characteristic shows constant resistances for all chosen admixtures with the resistances of the admixtures of 0.5% and 1% being the same. The resistance of the lowest oxygen admixture is observed to be different from the other cases which was attributed to a lack of oxygen in this plasma. In order to check which is the lowest oxygen admixture that does not cause a change in the resistance, it is proposed to perform further measurements with oxygen admixtures ranging from 0.25% to 0.5%.

The density trends of the different oxygen admixtures showed the same trends for plasma powers below 2 W. In case of the lowest admixture is was observed that more than 2 W of plasma power could not be deposited in the oxidation of methane. Therefore, it is proposed that future experiments should be performed with an oxygen admixture of at least 0.5% in order not to restrict the plasma chemistry by a lack of oxygen.

The amounts of carbon and hydrogen bond in other products than the analysed species are determined to be in the order of 10% and 25%, respectively. As no dependency of the amount on the plasma power was observed future studies can be performed regardless on the plasma power within the examined region. While the whole carbon is expected to be bond in intermediate products, the assumption that H_2 was formed is made. In order to examine how much H_2 is formed, future experiments should be performed with an additional measurement of molecular hydrogen.
The main reaction of the plasma chemistry was derived to:

$$CH_4 + 2\,O_2 \rightarrow CO + X \rightarrow CO_2 + 2\,H_2O$$

on base of the observed densities and balances.

The reconstruction of this reaction using a global chemistry model yielded proper results for most of the species. For further modelling using the global model, the CO_2 conversion should be implemented based on densities of He^* obtained from additional measurements.

The linear correlation between plasma power and electron density was ascribed to the formation of O^--ions whose density is expected to vary with oxygen admixture. It is proposed that further studies with the aim of measuring the density of O^--ions are performed to strengthen this assumption.

In this study slopes for three different oxygen admixtures were determined whose values are non-linear with the oxygen admixture. If slopes for other than the chosen oxygen admixtures were determined, a correlation of admixture A and slope $s(A)$ could be derived. Assuming a linear dependency on the plasma power in all cases, a correlation between the electron density $n(e)$ and the plasma power P_{Pl} of the following form could be deduced:

$$n_e(A, P_{pl}) = s(A) \times P_{Pl}$$

With this equation the electron density of a plasma with measured plasma power could be calculated directly without performing any additional measurements. Furthermore, it would be possible to replace the parameter electron density within the global model by the parameters admixture and plasma power which are more easy to measure. This could enable a more direct connection between experiment and theory, allowing theoretical predictions for further studies.

As the formation of O^--ions is expected to occur within every reactive plasma which contains oxygen atoms, the here presented method of analysis of the electron density can be extended to other oxygen containing plasmas.

6. Conclusion

The calculation of absorption spectra of methane was used to analyse the plasma chemistry of helium non-equilibrium plasmas with different admixtures of CH_4 and O_2. During this analysis the rotational and vibrational temperatures of methane as well as density trends with respect to the plasma power were examined. Based on the analysis of different species a reaction of the plasma chemistry was derived and confirmed using a global chemistry model. By comparison of the global model to the measurements a coherence between electron density and plasma power was deduced.

Due to the used optical setup a density correction was performed yielding a setup specific correction factor of 0.78 ± 0.03. Based on this correction factor total internal reflections were deduced to be the main reason of a misestimate of the density.

In order to verify the calculated absorption spectra measurements with a generator power of 50 W were performed. The rotational temperature was estimated to be in the order of 370 K, the expected temperature of the plasma chamber. The vibrational bending temperatures T_{vib2} and T_{vib4} were observed to be in the same temperature realm due to the small momentum transfer in collisions with electrons. The vibrational stretching temperatures T_{vib1} and T_{vib3} were measured to be in the region of 1000 K, due to electron impact excitation.
The plasma chemistry in plasmas with a pure CH_4 admixture was restricted to the formation of other hydrocarbons than CH_4 with comparable small densities. Due to a lack of observations a coating of the plasma chamber was precluded.

The plasma power was determined using a VI-probe, yielding plasma powers ranging from 0.75 W to 3.5 W. The correlation between generator power and plasma power in case of plasmas with oxygen and methane admixtures was observed to be linear in all cases. Plasmas of oxygen admixtures of 0.5% and 1% showed the same trend, implying an equal electrical behaviour. The plasma power of plasmas of an oxygen admixtures of 0.25% showed a less steep behaviour with respect to generator power which was attributed to a lack of oxygen in those plasmas.

Density trends within plasmas of different oxygen admixtures showed similar behaviours up to a plasma power of 2 W. Plasmas of admixtures of 0.5% and 1% showed the same behaviour for all observed plasma powers, indicating that enough oxygen for the inserted amount of methane was provided. Based on the case of 0.25% of oxygen admixture it was derived that 2 W of plasma power are sufficient so that the vast majority of methane reacts in case of methane and oxygen admixtures of 0.25%.

The amount of carbon and hydrogen bond in other than the measured products was estimated to 10% and 25%, respectively. In case of carbon, intermediate products are expected to caused this deficit, whereas hydrogen is expected to be present in its molecular form as well. In both cases, the amount of intermediate products was independent on the plasma power.
The main reaction of plasma chemistry in the observed plasma was:

$$CH_4 + 2\,O_2 \rightarrow CO + X \rightarrow CO_2 + 2\,H_2O$$

This reaction was confirmed by the use of a global chemistry model with the density of CO not matching. The given explanation for this was the missing implementation of

CO_2 dissociation. Problems with the chemical model occurred in cases of high oxygen admixtures as the methane was consumed entirely.
From the comparison of global model and measurement linear correlations between the electron density and the plasmas power were obtained. The different behaviours of the electron densities of the plasmas of different oxygen admixtures with respect to the plasma power were explained by the formation of O^--ions from free electrons and oxygen radicals. These lead to a lower electron density in cases of higher oxygen admixtures.

The calculation of absorption spectra of methane provides an accurate method of analysis of methane in non-equilibrium plasmas. It can either be used to calibrate a setup or to monitor the density and temperatures of methane. From these informations, statements about the different excitation mechanisms present in the plasma can be deduced.
Together with absorption spectra of other molecules, it provides a powerful method to monitor plasma chemistry. The comparison of the measurements with a global chemistry model allows predictions for not measured plasma parameters.

Acknowledgement

Zum Schluss möchte ich mich bei folgenden Personen bedanken:

- Prof. Dr. Achim von Keudell für die Beantwortung jedweder aufkommender Fragen und die Bereitstellung des globalen Modells.
- Theresa Urbanietz für die Betreuung und fleißiges Korrekturlesen.
- Allen Beteiligten des Dienstagsmeetings, allen voran Dr. Marc Böke, für stets konstruktives feedback zu präsentierten Daten.
- Den anderen Bachelorstudenten, die stets für eine entspannte Stimmung gesorgt haben.

Zudem möchte ich meiner Familie danken, die mich während des gesammten Studiums unterstützt hat.

Bibliography

[1] John FB Mitchell. "The "greenhouse" effect and climate change". In: *Reviews of Geophysics* 27.1 (1989), pp. 115–139.

[2] T Urbanietz et al. "Non-equilibrium excitation of CO2 in an atmospheric pressure helium plasma jet". In: *Journal of Physics D: Applied Physics* 51.34 (2018).

[3] Andrew PE York, Tiancun Xiao, and Malcom LH Green. "Brief overview of the partial oxidation of methane to synthesis gas". In: *Topics in Catalysis* 22.3-4 (2003), pp. 345–358.

[4] LM Zhou et al. "Partial oxidation of methane to methanol with oxygen or air in a nonequilibrium discharge plasma". In: *Plasma Chemistry and Plasma Processing* 18.3 (1998), pp. 375–393.

[5] MJ Brown and ND Parkyns. "Progress in the partial oxidation of methane to methanol and formaldehyde". In: *Catalysis Today* 8.3 (1991), pp. 305–335.

[6] Wei Liu and Maria Flytzanistephanopoulos. "Total oxidation of carbon monoxide and methane over transition metal fluorite oxide composite catalysts: I. Catalyst composition and activity". In: *Journal of Catalysis* 153.2 (1995), pp. 304–316.

[7] Delphine Roth et al. "Catalytic behaviour of Cl-free and Cl-containing Pd/Al2O3 catalysts in the total oxidation of methane at low temperature". In: *Applied Catalysis A: General* 203.1 (2000), pp. 37–45.

[8] B L M Klarenaar et al. "Time evolution of vibrational temperatures in a CO 2 glow discharge measured with infrared absorption spectroscopy". In: *Plasma Sources Science and Technology* 26.11 (2017).

[9] Francis F Chen. *Introduction to plasma physics*. Springer, New York, 1974.

[10] Mansel Davies et al. *Infra-red spectroscopy and molecular structure*. New York, 1963.

[11] Gerhard Herzberg. *Infrared and Raman spectra of polyatomic molecules*. D. Van Nostrand Company.; New York, 1945.

[12] Gerhard Herzberg. *Molecular spectra and molecular structure. Vol. 1: Spectra of diatomic molecules*. 1950.

[13] Peter Atkins, Julio De Paula, and James Keeler. *Atkins' physical chemistry*. Oxford university press, 2018.

[14] Gerhard Herzberg. *Molecular spectra and molecular structure. Vol. 3: Electronic spectra and electronic structure of polyatomic molecules*. 1966.

[15] Arindam Chakraborty et al. "Calculation of converged rovibrational energies and partition function for methane using vibrational–rotational configuration interaction". In: *The Journal of chemical physics* 121.5 (2004), pp. 2071–2084.

[16] Iouli E Gordon et al. "The HiTRAN2016 molecular spectroscopic database". In: *Journal of Quantitative Spectroscopy and Radiative Transfer* 203 (2017), pp. 3–69.

[17] E. Bright Wilson. "The Statistical Weights of the Rotational Levels of Polyatomic Molecules, Including Methane, Ammonia, Benzene, Cyclopropane and Ethylene". In: *The Journal of Chemical Physics* 3.5 (1935), pp. 276–285.

[18] James T Yardley and C Bradley Moore. "Vibrational energy transfer in methane". In: *The Journal of Chemical Physics* 49.3 (1968), pp. 1111–1125.

[19] Laurence S Rothman et al. “The HiTRAN 2004 molecular spectroscopic database”. In: *Journal of Quantitative Spectroscopy and Radiative Transfer* 96.2 (2005), pp. 139–204.

[20] George Socrates. *Infrared and Raman characteristic group frequencies: tables and charts*. John Wiley & Sons, 2004.

[21] W Tsang and RF Hampson. “Chemical kinetic data base for combustion chemistry. Part I. Methane and related compounds”. In: *Journal of Physical and Chemical Reference Data* 15.3 (1986), pp. 1087–1279.

[22] lxcat.net. *Morgan Kinema Research & Software*. 2018. URL: `www.lxcat.net/Morgan` (visited on 09/20/2018).

[23] D.G. Keil et al. “Rate Constants for the Reaction of Ground State Atomic Oxygen with Methanol”. In: *Journal of Chemical Physics* 75 (1981).

[24] Wing Tsang. “Chemical kinetic data base for combustion chemistry. Part 2. Methanol”. In: *Journal of physical and chemical reference data* 16.3 (1987), pp. 471–508.

[25] J. A. Manion et al. *NIST Chemical Kinetics Database, NIST Standard Reference Database 17*. 2018. URL: `http://kinetics.nist.gov/` (visited on 09/17/2018).

[26] H. Grotheer et al. “Non-arrhenius behavior of the reaction of hydroxymethyl radicals with molecular oxygen”. In: *The Journal of Physical Chemistry* 92 (1988).

[27] J.C. Tully. “Reactions of O(1D) with atmospheric molecules”. In: *Journal of Chemical Physics* 62 (1975).

[28] V. Lissianski et al. “High-temperature measurements of the rate of the coefficient of the H + CO2 -> CO + OH reaction”. In: *Chemical Physics Letters* 240 (1995), pp. 57–62.

[29] X.Q. You et al. “Reaction kinetics of CO+HO2 -> products: Ab initio transition state theory study with master equation modeling”. In: *The Journal of Physical Chemistry A* 111 (2007), pp. 4031–4042.

[30] Plasma Data Exchange Project. *LXcat*. 2018. URL: `https://fr.lxcat.net/data/set_type.php` (visited on 09/17/2018).

A1. Data

Table A1.1: Degeneracies of the ro-vib levels of CH_4 following Wilson [17] without the space degeneracy factor $(2j+1)$, $n \in \mathbb{N}_0$

		$J = 6n$	$J = 6n+1$	$J = 6n+2$
Nuclear Quintet	A	$5\left(\frac{J}{6}+1\right)$	$5\left(\frac{J-1}{6}\right)$	$5\left(\frac{J-2}{6}\right)$
Nuclear Singlet	E	$\left(\frac{J}{3}\right)$	$\left(\frac{J-1}{3}\right)$	$2\left(\frac{J-2}{6}+1\right)$
Nuclear Triplet	F	$9\left(\frac{J}{6}\right)$	$3\left(\frac{J-1}{2}+1\right)$	$3\left(\frac{J-2}{2}+1\right)$
		$J = 6n+3$	$J = 6n+4$	$J = 6n+5$
Nuclear Quintet	A	$5\left(\frac{J-3}{6}+1\right)$	$5\left(\frac{J-4}{6}+1\right)$	$5\left(\frac{J-5}{6}\right)$
Nuclear Singlet	E	$\left(\frac{J-3}{3}\right)$	$2\left(\frac{J-4}{6}+1\right)$	$2\left(\frac{J-5}{6}+1\right)$
Nuclear Triplet	F	$3\left(\frac{J-3}{2}+2\right)$	$3\left(\frac{J-4}{2}+2\right)$	$3\left(\frac{J-5}{2}+3\right)$

Table A1.2: Constants for the different species provided by HiTRAN [16].

Species	CH_4	H_2O	CO_2	CO
Quantum class	10	10	5	1
Vibrational modes number	4	3	3	1
Vibrational modes frequencies	2917	3656.65	1333.93	2143.24
cm^{-1}	1533	1594.59	667.47	
	3018.9	3755.79	2349.16	
	1306			
Vibrational modes maximal	40	40	40	35
numbers of states	40	40	70	
	30	30	30	
	30	30		
Vibrational modes centrifugal	0.001	0.001	2.93	13.29
constants	0.001	0.001	-0.38	
cm^{-3}	0.001	0.001	12.47	
	0.001	0.001		
Rotational modes constants				
$B(cm^{-1})$	5.241	26.608	0.39022	1.9225
$D(10^{-6}cm^{-1})$	0.0	14.672	0.1333	6.121
$H(10^{-12}cm^{-1})$	0.0	9.457	0.0090	5.7
Isotopical abundance first three	0.984	1.000	0.984	0.984
	0.01105	0.00	0.01105	0.01105
	0.00	0.00	0.00	0.00

Table A1.3: The format of transition information used in HiTRAN [19].

Parameter	Meaning	Field Length
M	Molecule number	I2
I	Isotopologue number	I1
ν	wavenumber	F12
S	Intensity	F10
R	Transition Moment	F10
A	Einstein coefficient	F10
γ_{air}	Air broadening half width	F5
γ_{self}	Self broadening half width	F5
E''	Lower state energy	F10
n_{air}	Temperature exponent	F4
δ_{air}	Pressure shift	F4
V'	Upper state quanta	I15
V''	Lower state quanta	I15
Q''	Upper state local quanta	I15
Q'	Lower state local quanta	I15
I_{err}	Uncertainty indices	I6
I_{ref}	Reference indices	I12
	Flag	I1
g''	Statistical weight upper state	I7
g'	Statistical weight lower state	I7

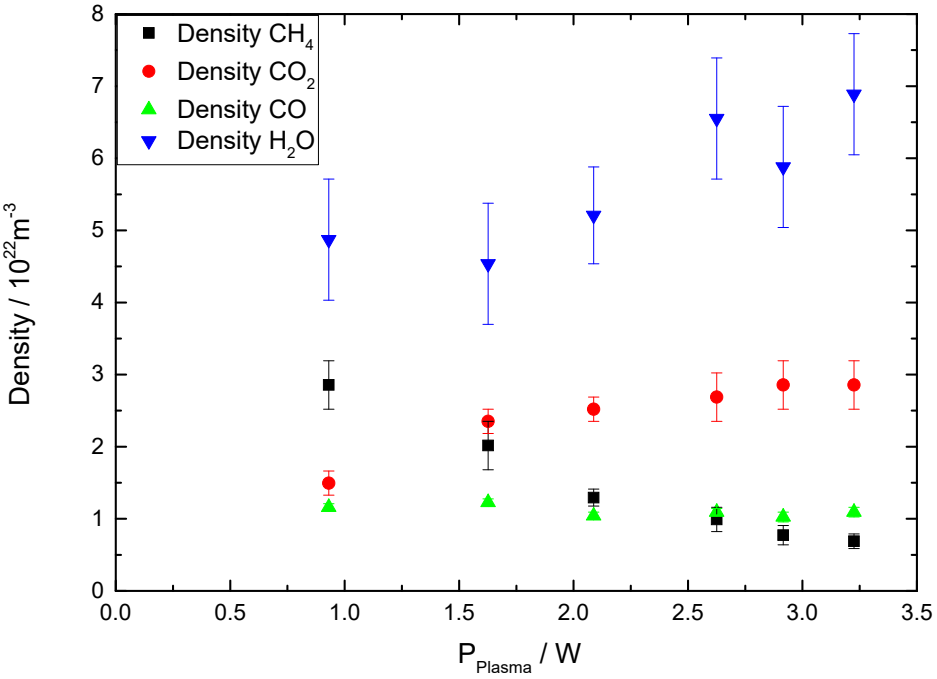

Figure A1.1: Determined densities for the different species in case of an oxygen admixture of 0.5%.

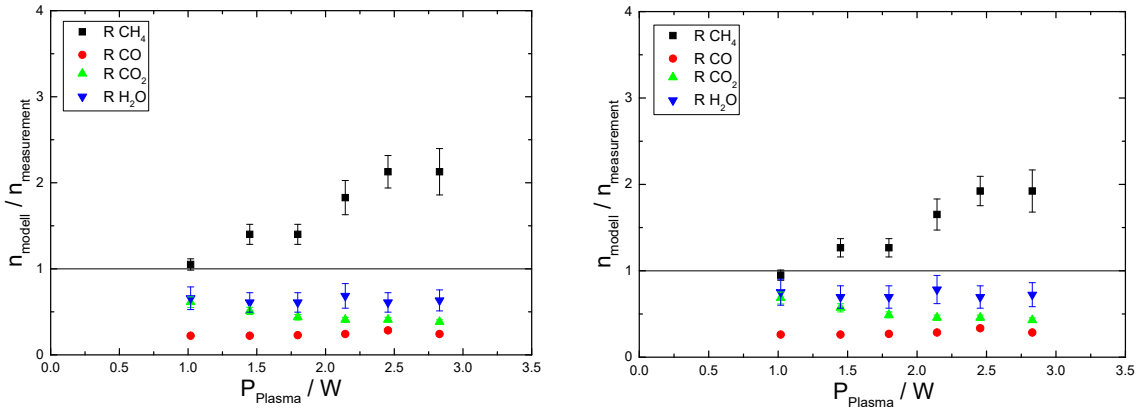

(a) $n_e = 2.0 \times 10^{16}\,\mathrm{m}^3$

(b) $n_e = 2.5 \times 10^{16}\,\mathrm{m}^3$

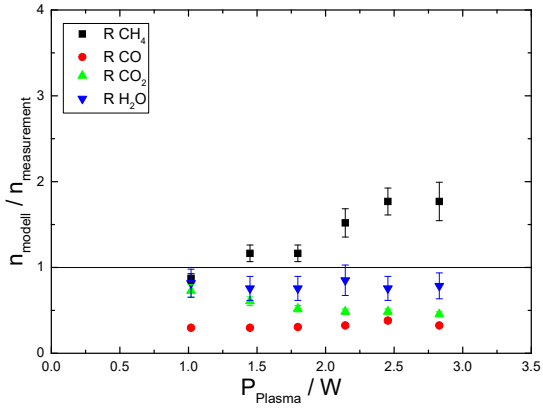

(c) $n_e = 3.0 \times 10^{16}\,\mathrm{m}^3$

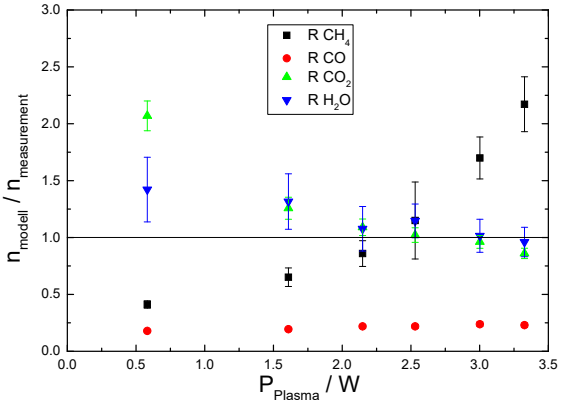

(d) $n_e = 1.0 \times 10^{16}\,\mathrm{m}^3$

Figure A1.2: Ratios of modelled densities to determined densities. A1.2a to A1.2c refer to an oxygen admixture of 0.25%, A1.2d to an admixture of 1%.

A2. Global model

The chemistry happening in a plasma can be understood by the use of global chemistry models, which describe occurring chemical reactions based on their reaction rates and given initial parameters. In general, chemical reactions from reagents to products are described by:

$$\sum_{i}^{N_i} r_i R_i \rightarrow \sum_{j}^{N_j} p_j P_j \tag{A2.1}$$

with the numbers of reagents and products N_i and N_j, respectively, the amount of reagent R_i, r_i, and the amount of product P_j, p_j. In this consideration, no back-reactions are taken into account. From the change in reactants and products, differential equations describing their formation and loss can be derived:

$$\frac{dn_{R_i}}{dt} = -k \prod_{i}^{N_i} n_{R_i} \tag{A2.2}$$

$$\frac{dn_{P_j}}{dt} = k \prod_{j}^{N_j} n_{P_j} \tag{A2.3}$$

with the density of a species n and the rate coefficient k. The given reactions describe chemical reactions of an ensemble of particles in an infinite volume with a fixed density. In order to take a look at a finite volume, in- and outflow have to be taken into account. The inflow of a species A into a volume V changes the density of the species n_A like:

$$\frac{dn_A}{dt} = \frac{\Phi_{in}}{V} \tag{A2.4}$$

with the inflow of the species Φ_{in}. With a higher density, the pressure inside the volume increases. In order to keep the pressure constant, the outflow of a species B is described by:

$$\frac{dn_B}{dt} = -\frac{n_B}{\tau} \tag{A2.5}$$

with the density of the species n_B and the mean residence time of any molecule τ. The residence time τ is calculated from the ratio $\frac{V}{\Phi_{all}}$, based on the volume V and the total inflow of species Φ_{all}.

In order to calculated reaction rates, the electron energy distribution function needs to be known. As the pressure of the system is high, it is reasonable to assume a normalized Maxwell distribution:

$$p(E,T) = \frac{2}{\sqrt{\pi}} T^{-3/2} \sqrt{E} e^{-\frac{E}{T}} \tag{A2.6}$$

with the electron temperature T and the energy E in the same unit. This Maxwell distribution differs from the one given in equation 2.24 as an ensemble of particles is described. The rate coefficient is obtained by the integral of the product of EEDF, mean velocity v, and cross section σ. Replacing the velocity by the energy, using the classical relation $E = \frac{v^2}{2m}$, yields:

$$k = \sqrt{\frac{2e}{m}} \frac{2}{\sqrt{\pi}} T^{-3/2} \int_0^\infty \sigma E e^{-\frac{E}{T}} dE \tag{A2.7}$$

with the temperate T and energy E in units of electron volts, respectively, the elemental charge e, and the mass of the particle m. With a given cross section, this expression is used to calculate reaction rates for a given energy E. The calculated rates for the used reactions are displayed in table 5.1.

The time intervals of calculation are set to 1×10^{-8} s. From the calculations, partial pressures for the different species at the chosen time steps are obtained.